The zero-multipole summation method for estimating electrostatic interactions in molecular dynamics: Analysis of the accuracy and application to liquid systems

Ikuo Fukuda, Narutoshi Kamiya, and Haruki Nakamura

Citation: The Journal of Chemical Physics **140**, 194307 (2014); doi: 10.1063/1.4875693
View online: http://dx.doi.org/10.1063/1.4875693
View Table of Contents: http://scitation.aip.org/content/aip/journal/jcp/140/19?ver=pdfcov
Published by the AIP Publishing

The zero-multipole summation method for estimating electrostatic interactions in molecular dynamics: Analysis of the accuracy and application to liquid systems

Ikuo Fukuda,[1,2,a)] Narutoshi Kamiya,[1] and Haruki Nakamura[1]
[1]*Institute for Protein Research, Osaka University, 3-2 Yamadaoka, Suita, Osaka 565-0871, Japan*
[2]*RIKEN (The Institute of Physical and Chemical Research), 2-1 Hirosawa, Wako, Saitama 351-0198, Japan*

(Received 16 December 2013; accepted 29 April 2014; published online 20 May 2014)

In the preceding paper [I. Fukuda, J. Chem. Phys. **139**, 174107 (2013)], the zero-multipole (ZM) summation method was proposed for efficiently evaluating the electrostatic Coulombic interactions of a classical point charge system. The summation takes a simple pairwise form, but prevents the electrically non-neutral multipole states that may artificially be generated by a simple cutoff truncation, which often causes large energetic noises and significant artifacts. The purpose of this paper is to judge the ability of the ZM method by investigating the accuracy, parameter dependencies, and stability in applications to liquid systems. To conduct this, first, the energy-functional error was divided into three terms and each term was analyzed by a theoretical error-bound estimation. This estimation gave us a clear basis of the discussions on the numerical investigations. It also gave a new viewpoint between the excess energy error and the damping effect by the damping parameter. Second, with the aid of these analyses, the ZM method was evaluated based on molecular dynamics (MD) simulations of two fundamental liquid systems, a molten sodium-chlorine ion system and a pure water molecule system. In the ion system, the energy accuracy, compared with the Ewald summation, was better for a larger value of multipole moment l currently induced until $l \lesssim 3$ on average. This accuracy improvement with increasing l is due to the enhancement of the excess-energy accuracy. However, this improvement is wholly effective in the total accuracy if the theoretical moment l is smaller than or equal to a system intrinsic moment L. The simulation results thus indicate $L \sim 3$ in this system, and we observed less accuracy in $l = 4$. We demonstrated the origins of parameter dependencies appearing in the crossing behavior and the oscillations of the energy error curves. With raising the moment l we observed, smaller values of the damping parameter provided more accurate results and smoother behaviors with respect to cutoff length were obtained. These features can be explained, on the basis of the theoretical error analyses, such that the excess energy accuracy is improved with increasing l and that the total accuracy improvement within $l \leq L$ is facilitated by a small damping parameter. Although the accuracy was fundamentally similar to the ion system, the bulk water system exhibited distinguishable quantitative behaviors. A smaller damping parameter was effective in all the practical cutoff distance, and this fact can be interpreted by the reduction of the excess subset. A lower moment was advantageous in the energy accuracy, where $l = 1$ was slightly superior to $l = 2$ in this system. However, the method with $l = 2$ (viz., the zero-quadrupole sum) gave accurate results for the radial distribution function. We confirmed the stability in the numerical integration for MD simulations employing the ZM scheme. This result is supported by the sufficient smoothness of the energy function. Along with the smoothness, the pairwise feature and the allowance of the atom-based cutoff mode on the energy formula lead to the exact zero total-force, ensuring the total-momentum conservations for typical MD equations of motion. © *2014 AIP Publishing LLC*. [http://dx.doi.org/10.1063/1.4875693]

I. INTRODUCTION

To understand the physical properties of a matter via an atomic level, molecular dynamics (MD) simulation is a powerful tool and has been widely used in computational studies. Even for details inaccessible to experiments, it enables us to, e.g., develop a new material in condensed matter or solve a molecular mechanism in a bimolecular system. In these simulations, the electrostatic interactions among charged particles play essential roles in a number of systems, with maintaining physical structures, generating chemical properties, and performing biological functions.[1–3] Thus, the accurate evaluations of the electrostatic interactions are important.

As well as the accuracy in the evaluations, a low computational cost is necessary for them. This is because almost all the cost is paid for this evaluation in a molecular simulation, including a classical MD study. In fact, such a cost is essentially proportional to N^2, the square of the number of the particles in a target classical system, in contrast to the short range interactions for which the cost is proportional to N. This yields a bottleneck of the simulations as the system size becomes large.

a)Electronic mail: ifukuda@protein.osaka-u.ac.jp

In this computational viewpoint, a cutoff-based (CB) approach is appealing, since it would give $O(N)$ scheme for a larger system, whereas it seems to be qualitatively different from the lattice sum (LS) approach. The latter, such as the Ewald method[4,5] or its variations, has been used as a standard in molecular simulations,[6] under the assumption of the periodic boundary condition (PBC). PBC allows us to mimic a bulk state, avoiding the creation of an interface, which often causes significant artifacts in simulations. However, since the evaluation under the PBC includes infinitely many interactions in principle, the computational cost should not be small in general. Of course, a computational inefficient feature of the conventional LS method has been eliminated in considerable extent, using, e.g., a mesh-based approach,[7,8] but this does not necessarily mean the dead-end of developing other methodological ideas and algorithms. In fact, it is useful to develop a method appropriate for a non-periodic system and construct a very simple algorithm applicable easily to any computational architectures.

Again, CB approaches are appealing in such viewpoints that they are irrelevant to the boundary conditions in general and that these local interaction approaches enable us to easily design parallel algorithms. The most critical issues of this approach are, however, to improve the accuracy and remove the possible artifacts. In fact, artifacts have been found in a number of studies,[1,9] including ion systems,[10] a water system,[11] and a protein-water system.[12] For this reason, and because maintaining the accuracy is a severe issue, many researchers may have avoided using these approaches. However, quite recently, it has been understood that the artifacts of the CB approach can be sufficiently minimized if suitable devices are applied. Such devices capture certain specific features in the set of charged particles, e.g., a symmetry of the system, a system-environment interaction, and electrostatic neutrality. They lead to modifications of the pair potential function, from the bare Coulombic form to the other forms.

Such a CB approach, often termed a non-Ewald approach,[13] includes a number of methods. In the reaction field method,[14,15] the effect outside the cutoff sphere is included via interactions between dipoles made in the sphere and an electric field generated by polarized dielectric continuum outside the sphere, which is assumed to be described by a homogeneous dielectric constant. This additional interaction can be represented by a very simple pairwise formula. Despite this device, both its effectiveness and artifacts have been pointed out during its long history.[16–22] However, the artifact can be diminished if we use additional devices such as an atomic-based cutoff mode and a high dielectric constant.[13,23] Furthermore, against the homogeneity assumption, the effectiveness has recently been realized in inhomogeneous systems.[24,25]

The pre-averaging CB method[26] was introduced by Yakub and Ronchi in order to remove the artificial cubic symmetry in the LS method. The energy formula was obtained by averaging the quantities over spherical angular coordinates in the Ewald summation expansion, and this pre-average gave simple pairwise expression using the cutoff length that is the radius of the volume-equivalent sphere of the cubic MD cell.[26,27] This method has been very successfully applied to crystal systems,[26,28] disordered systems,[28–30] and inhomogeneous systems.[31]

Likewise, rather than the cubic periodicity in the LS method, the isotropic periodic summation, proposed by Wu and Brooks,[32,33] assumes the isotropic periodicity, which comes from the images of the local region statistically distributed in an isotropic and periodic manner. The resulting energy formula is expressed by a pairwise form. The point distinguishable from other CB methods is that it can be applied not only to the Coulombic function but also to other functions including the van der Waals (vdW) potential function. This method and its extension[34] have been successfully applied to bulk waters,[35] aqueous solvation of ions,[36] lipid bilayers and monolayers,[37] and used for constructing force fields.[38–40]

Wolf *et al.*[41,42] found that the energy error in the straight cutoff is nearly proportional to the net charge in the cutoff sphere. The subtraction of these excess charge contributions formalizes a simple pairwise formula for conducting the zero-charge (ZC) CB scheme. They also revealed the importance of the damping effect for the pair potential function to accelerate the efficiency. The efficiency of the method of Wolf *et al.* in terms of the accuracy and computational cost has been demonstrated and utilized in many studies (see Ref. 13 and the references therein; also see Refs. 43–52 for recent progress).

The force-matching method[53,54] concentrates on the effectiveness of the final form of the energy or force function. It has recently been used for a new generation of coarse-grained potentials that account for a simplified electrostatic description of soluble proteins.[55] Other important non-Ewald electrostatics methods have been developed, including the single sum technique,[56] local molecular field theory,[57] the fast multipole method,[58,59] a fast multipole method combined with a reaction field,[60] the lattice-sum-emulated reaction-field method,[61] an image-charge reaction field method,[62,63] and a model of electrostatic and liquid-structure forces.[64]

On the basis of the development of the ZC principle,[42,65–71] the zero-dipole (ZD) summation method[72] provides the energy derived by counting the interactions for a neutralized subset regarding the dipoles as well as the charges. This summation prevents the electrically non-neutral dipole states that may artificially be generated by a simple cutoff truncation, which often causes significant artifacts. It has been applied to several systems,[72–76] and provided more accurate electrostatic energies than the ZC scheme. A further developed scheme was proposed to reach more accurate results. This scheme extends the viewpoint of the summation over a neutralized subset in order to take into account a multipole moment up to any order. The formalism, named zero-multipole (ZM) method,[77] gives a more accurate pairwise sum expression of the excess energy, compared with the ZD method, as long as the physical states admit the description of the zero-multipole principle.

Aside from the potentiality on the computational cost, a new CB method should be investigated in detail foremost from the point of the accuracy. For the ZM method, general theoretical discussions and a basic numerical consideration on typical solid states were done in the previous

paper.[77] In this paper, we investigate the accuracy of the ZM method applying to liquid states for two systems, which are prototypic in molecular simulations. The first one is a sodium chloride liquid (molten) system within a strongly-coupled regime, where the Coulombic interaction governs the global description of the system. The second system is a liquid of pure water molecules, which are neutralized but polar molecules, and provides the basis of the biomolecular systems. In these systems, we first examine the effect of both the cutoff length and the damping parameter on the accuracy. Second, we study the effect of the multipole moment l newly provided by the current method. Furthermore, since such a parameter-value dependence and a target-matter dependence are not necessarily simply understandable in realistic applications, we provide a theoretical analysis of the error in the current method. The error is divided into three components, and the parameter dependencies are investigated for an individual component. Utilizing the isotropic properties of liquid states helps us to promote such theoretical analyses. These analyses are also useful to seek a good assignment of the parameter values.

In Sec. II A, we first briefly review the ZM summation method. After discussing the background and a physical motivation of the method, we demonstrate technical points that are required in Secs. III–V, on the emphasis of their physical interpretations. In particular, we state the notions of zero-multipole state and show the excess energy representation via a polynomial which is related to the excess energy error. In Sec. II B, we currently propose a specific protocol for applying the ZM method to general molecular systems. In Sec. III, the theoretical error analyses are performed with the assumption of the isotropic condition of the target system that permits a continuous density approximation. We analyze the three components of the error and their parameter dependencies, and reconsider the damping effect via the damping parameter. Employing the numerical methods described in Sec. IV, we show the results of MD simulations using the ZM schemes applied to a molten NaCl ion system and a bulk water molecular system in Sec. V. Accuracies, stabilities, and applicability of the method are discussed by investigating energy accuracies, conservation laws, and structural properties of the systems. The characteristic features of the method are analyzed by clarifying the parameter dependencies on the basis of the discussions in Sec. III and by comparing with conventional methods. We conclude with remarks in Sec. VI.

II. ZERO-MULTIPOLE SUMMATION METHOD

A. Background and formula

Although the Coulombic interaction is long-ranged in principle, as long as we consider a condensed phase such as in realistic materials and biophysical environment, its effect is screened or hindered by the charge cancellation in practice. In this point of view, the cutoff approach for evaluating the interactions is not wrong fundamentally. However, if one takes simply the straight-cutoff procedure, the particle configuration inside this purely distance-judged cutoff sphere does not capture such a charge-neutralized state in general. This fact explains the observation such that the straight cutoff often exhibits physical instability, causes significant artifacts, and generates noise in evaluating the energy.

Thus, the interactions should be counted for a certain neutralized subset of charges as for individual particles, instead of counting all the particles in a given cutoff sphere. We consider that for equilibrated configurations observed in, e.g., a physically stable system, neutrality of lth moment multipoles, as well as charges (0th moment multipoles), is attained (approximately) even in a local level, and this physical information should be taken into account to evaluate the interactions.[77] For such a state, a summation method that reflects this neutrality condition promises to provide a good approximation to estimate the energy. In fact, in the ZD method,[72] which corresponds to the ZM method with the multipole moment of $l = 1$, its accuracy has been shown in actual numerical simulations for ion systems,[72] a bulk water system,[73] a membrane protein system with explicit membrane and solvent molecules and ions,[74] and a double-stranded DNA with explicit water and ions.[75]

The neutrality condition in the ZM method for N particles with charges $(q_1, \ldots, q_N)$ and configurations $x \equiv (x_1, \ldots, x_N)$ is specifically represented as follows: for any particle $i \in \mathcal{N} \equiv \{1, \ldots, N\}$, there exists a neutralized subset $\mathcal{M}_i^{(l)} \subset \mathcal{N}_i \equiv \mathcal{N} - \{i\}$ such that

$$\forall j \in \mathcal{M}_i^{(l)}, \quad r_{ij} < r_c, \tag{1a}$$

$$\sum_{j \in \mathcal{M}_i^{(l)} \cup \{i\}} q_j = 0, \tag{1b}$$

$$\sum_{j \in \mathcal{M}_i^{(l)} \cup \{i\}} q_j x_j = 0, \tag{1c}$$

$$\cdots$$

$$\sum_{j \in \mathcal{M}_i^{(l)} \cup \{i\}} q_j x_j \otimes \overset{l}{\cdots} \otimes x_j = 0, \tag{1d}$$

$$\forall j \in \mathcal{N}_i - \mathcal{M}_i^{(l)} \ (r_{ij} < r_c \Rightarrow r_{ij} \simeq r_c), \tag{1e}$$

where $r_{ij} \equiv \|x_{ij}\|$ is the distance of particles i and j (viz., $x_{ij} \equiv x_i - x_j$ describes a 3-dimensional vector), and r_c is the cutoff length for the interactions. These conditions mean that: (a) all particles in $\mathcal{M}_i^{(l)}$ are inside the cutoff sphere; (b) the sum of the charges in the neutralized subset adding the target particle i, $\mathcal{M}_i^{(l)} \cup \{i\}$, becomes zero [viz., the neutrality holds on $\mathcal{M}_i^{(l)} \cup \{i\}$, but for convenience, i is defined to be not involved in $\mathcal{M}_i^{(l)}$]; (c) the sum of the dipoles in $\mathcal{M}_i^{(l)} \cup \{i\}$ is zero; the other conditions up to (d), which are represented by higher order tensors, require the vanishing of mth multipoles in $\mathcal{M}_i^{(l)} \cup \{i\}$ for $m = 0, \ldots, l$ [viz., the conditions of $m = 0$ and 1 correspond to conditions (1b) and (1c), respectively]; and (e) any particle (except i) not belonging to $\mathcal{M}_i^{(l)}$ but inside the cutoff sphere are located near the cutoff surface (see Fig. 1). We often refer to x as a (lth) *ZM state*.

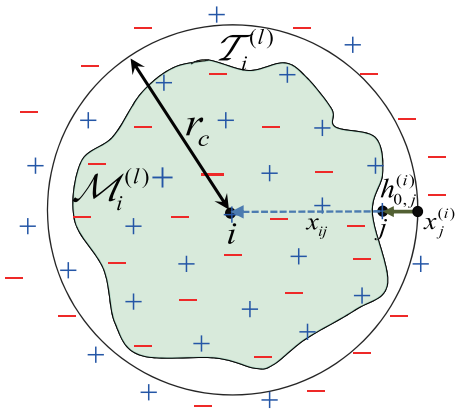

FIG. 1. The straight cutoff truncation takes into account all charges in a given cutoff sphere with a radius r_c centered about particle i. The current zero-multipole summation method conceptually deals with the particles only in the shaded region, which schematically represent the zero lth multipole subset $\mathcal{M}_i^{(l)}$. The particles in the non-shaded region are the members of an excess subset $\mathcal{J}_i^{(l)}$. Particle j at position x_j is one of the members of $\mathcal{J}_i^{(l)}$, and displacement vector $h_j^{(i)}$ is measured by the difference between x_j and its shifted position. The originally given displacement vector is $h_{0,j}^{(i)}$, and the shifted position of x_j, designated as $x_j^{(i)}$, is at the cutoff surface along the vector $x_j - x_i$.

We calculate the total Coulombic energy $E(x)$ as follows:

$$E(x) = \frac{1}{2}\sum_{i\in\mathcal{N}}\sum_{j\in\mathcal{N}_i}\frac{q_iq_j}{r_{ij}} \tag{2a}$$

$$= \frac{1}{2}\sum_{i\in\mathcal{N}}\sum_{j\in\mathcal{N}_i} q_iq_jV(r_{ij}) + \frac{1}{2}\sum_{i\in\mathcal{N}}\sum_{j\in\mathcal{N}_i} q_iq_j\left[\frac{1}{r_{ij}} - V(r_{ij})\right] \tag{2b}$$

$$\approx \frac{1}{2}\sum_{i\in\mathcal{N}}\sum_{j\in\mathcal{M}_i^{(l)}} q_iq_jV(r_{ij}) - \frac{\alpha}{\sqrt{\pi}}\sum_{i\in\mathcal{N}} q_i^2. \tag{2c}$$

Here, for the decomposition in Eq. (2b) we have used

$$V(r) = \frac{\mathrm{erfc}(\alpha r)}{r}, \tag{3}$$

a Coulombic potential function with a damping factor $\mathrm{erfc}(\alpha r)$, complementary error function of αr, for which $\alpha \geq 0$ [note $V(r) = 1/r$ for $\alpha = 0$, the non-damping case]. In the first term of Eq. (2c) we have utilized the strategy, i.e., the replacement

$$\sum_{j\in\mathcal{N}_i} q_jV(r_{ij}) \to \sum_{j\in\mathcal{M}_i^{(l)}} q_jV(r_{ij}). \tag{4}$$

Namely, the contributions that should be counted are those from the *ZM subset* $\mathcal{M}_i^{(l)}$ for every i. In other words, we assume the approximation

$$\sum_{i\in\mathcal{N}}\sum_{j\in\mathcal{N}_i} q_iq_jV(r_{ij}) \approx \sum_{i\in\mathcal{N}}\sum_{j\in\mathcal{M}_i^{(l)}} q_iq_jV(r_{ij}). \tag{5}$$

The second term of Eq. (2b) can be read as

$$\frac{1}{2}\sum_{i\in\mathcal{N}}\sum_{j\in\mathcal{N}_i} q_iq_j\left[\frac{1}{r_{ij}} - V(r_{ij})\right] \tag{6a}$$

$$= \frac{1}{2}\sum_{i\in\mathcal{N}}\sum_{j\in\mathcal{N}}\frac{q_iq_j}{r_{ij}}\mathrm{erf}(\alpha r_{ij}) - \frac{1}{2}\lim_{r\to 0}\frac{\mathrm{erf}(\alpha r)}{r}\sum_{i\in\mathcal{N}} q_i^2 \tag{6b}$$

$$\sim -\frac{\alpha}{\sqrt{\pi}}\sum_{i\in\mathcal{N}} q_i^2 \ \text{ for small } \alpha, \tag{6c}$$

where we have used the fact that $\mathrm{erf}(\alpha r)$ is decreasing as decreasing the value of α, so that the first term of Eq. (6b) can be ignored for a small α. In fact, $\alpha = 0$ yields Eq. (6c) to be exact [viz., no-decomposition case in Eq. (2b)]. Our strategy is to use a small value of α.

From Eqs. (1a) and (2c) we get

$$E(x) \simeq \frac{1}{2}\sum_{i\in\mathcal{N}}\sum_{\substack{j\in\mathcal{N}_i \\ r_{ij}<r_c}} q_iq_jV(r_{ij}) - \hat{E}^{(l)}(x) - \frac{\alpha}{\sqrt{\pi}}\sum_{i\in\mathcal{N}} q_i^2, \tag{7}$$

where

$$\hat{E}^{(l)}(x) \equiv \frac{1}{2}\sum_{i\in\mathcal{N}}\sum_{j\in\mathcal{J}_i^{(l)}} q_iq_jV(r_{ij}), \tag{8}$$

with $\mathcal{J}_i^{(l)} \equiv \{j \in \mathcal{N}_i - \mathcal{M}_i^{(l)} \mid r_{ij} < r_c\}$, noting that $\sum_{j\in\mathcal{M}_i^{(l)}} = \sum_{j\in\mathcal{N}_i, r_{ij}<r_c} - \sum_{j\in\mathcal{J}_i^{(l)}}$. We call $\mathcal{J}_i^{(l)}$ an *excess subset*, which generates a non-zero multipole inside a given cutoff sphere. Here, $\hat{E}^{(l)}(x)$ is an *excess energy*, which should be removed from the energy that is evaluated on the simple cutoff truncation.

Excess energy can be approximated by a simple form with the accuracy of the lth degree with respect to displacement vector $h^{(i)} = (h_j^{(i)})$ (see Fig. 1), which can measure the size (smallness) of the excess subset $\mathcal{J}_i^{(l)}$, for all individual particles i. Namely, using condition (1) and a consistency condition regarding $\mathcal{J}_i^{(l)}$,[77] we have

$$\hat{E}^{(l)} = \check{E}^{(l)} + \Delta^{(l)}, \tag{9}$$

where

$$\check{E}^{(l)}(x) = \frac{1}{2}\sum_{i\in\mathcal{N}}\sum_{j\in\mathcal{J}_i^{(l)}} q_iq_jV_l(r_{ij}) \tag{10a}$$

$$= \frac{1}{2}\sum_{i\in\mathcal{N}}\sum_{\substack{j\in\mathcal{N}_i \\ r_{ij}<r_c}} q_iq_jV_l(r_{ij}) + \frac{1}{2}\sum_{i\in\mathcal{N}} q_i^2a_0^{(l)} \tag{10b}$$

is the approximation, and

$$\Delta^{(l)} \equiv \sum_{i\in\mathcal{N}} u_i \tag{11}$$

indicates the discrepancy described by the amplitude of the displacement vector such that

$$u_i(x^{(i)} + h^{(i)}) = o(\|h^{(i)}\|^l) \ \ (h^{(i)} \to 0). \tag{12}$$

Here,

$$V_l(r) \equiv \sum_{m=0}^{l} a_m^{(l)} r^{2m} \tag{13}$$

is a polynomial of distance r with coefficients $\{a_m^{(l)}\}$ (see Appendix A for detail), which are determined so that the following approximation of V by V_l at $r \sim r_c$ is valid:

$$V(r) - V_l(r) = o\left(|r - r_c|^l\right) \quad (r \to r_c). \tag{14}$$

The above formulae mean that the excess energy approximation becomes accurate as increasing l for a sufficiently small $h^{(i)}$. Such a smallness is ensured by condition (1e). Under the assumption that the replacement, Eq. (5), holds for a certain moment $l \equiv L$, we expect a more accurate energy expression for increasing l as long as $l \le L$. Note that the derivation of Eq. (10b) is equivalent to deriving the relation such that the contribution via the polynomial is zero on the union of $\{i\}$ and the neutralized subset, viz.,

$$\sum_{i\in\mathcal{N}} \sum_{j\in\mathcal{M}_i^{(l)}\cup\{i\}} q_i q_j V_l(r_{ij}) = 0, \tag{15}$$

which is proved from the zero multipole conditions and the consistency condition, as shown in Appendix C of Ref. 77.

From Eqs. (7)–(13), we have an approximation to $E(x)$, represented as

$$E_{\mathrm{ZM}}^{(l)}(x) \equiv \frac{1}{2} \sum_{i\in\mathcal{N}} \sum_{\substack{j\in\mathcal{N}_i \\ r_{ij}<r_c}} q_i q_j [V(r_{ij}) - V_l(r_{ij})] - \left[\frac{a_0^{(l)}}{2} + \frac{\alpha}{\sqrt{\pi}}\right] \sum_{i\in\mathcal{N}} q_i^2 \tag{16a}$$

$$= \frac{1}{2} \sum_{i\in\mathcal{N}} \sum_{\substack{j\in\mathcal{N}_i \\ r_{ij}<r_c}} q_i q_j [u^{(l)}(r_{ij}) - u^{(l)}(r_c)] - \frac{1}{2}\left[u^{(l)}(r_c) + \frac{2\alpha}{\sqrt{\pi}}\right] \sum_{i\in\mathcal{N}} q_i^2, \tag{16b}$$

where

$$u^{(l)}(r) \equiv V(r) - \sum_{m=1}^{l} a_m^{(l)} r^{2m} \tag{17}$$

[note $V(r_c) = V_l(r_c)$, so $a_0^{(l)} = u^{(l)}(r_c)$; see Eq. (14)] and its specific form is presented in Appendix A. Since $u^{(0)}(r) = V(r)$ and $u^{(1)}(r) = V(r) - (dV(r_c)/2r_c)r^2$, the scheme with $l = 0$ is equal to the method of Wolf *et al.*[42] and that with $l = 1$ is the ZD method.[72]

B. Application to general molecular system

For a classical molecular system, in general, we should evaluate

$$E^{(\mathrm{NB})}(x) \equiv \frac{1}{2} \sum_{i\in\mathcal{N}} \sum_{j\in\mathcal{N}_i - \mathcal{N}_i^{\mathrm{B}}} \frac{q_i q_j}{r_{ij}} \tag{18a}$$

$$= \frac{1}{2} \sum_{i\in\mathcal{N}} \sum_{j\in\mathcal{N}_i} \frac{q_i q_j}{r_{ij}} - \frac{1}{2} \sum_{i\in\mathcal{N}} \sum_{j\in\mathcal{N}_i^{\mathrm{B}}} \frac{q_i q_j}{r_{ij}}, \tag{18b}$$

where $\mathcal{N}_i^{\mathrm{B}}$ is the subset of particles that interact with particle i via bonding (bond, bend, torsion, etc.) interactions. As discussed in detail in the ZD scheme,[73] we apply the ZM scheme, Eq. (16b), to the first term in Eq. (18b). Thus,

$$E^{(\mathrm{NB})}(x) \simeq E_{\mathrm{ZM}(l)}^{(\mathrm{NB})}(x) \tag{19a}$$

$$\equiv E_{\mathrm{ZM}}^{(l)}(x) - \frac{1}{2} \sum_{i\in\mathcal{N}} \sum_{j\in\mathcal{N}_i^{\mathrm{B}}} \frac{q_i q_j}{r_{ij}} \tag{19b}$$

$$= \frac{1}{2} \sum_{i\in\mathcal{N}} \sum_{\substack{j\in\mathcal{N}_i \\ r_{ij}<r_c}} q_i q_j [u^{(l)}(r_{ij}) - u^{(l)}(r_c)] - \frac{1}{2} \sum_{i\in\mathcal{N}} \sum_{j\in\mathcal{N}_i^{\mathrm{B}}} q_i q_j \frac{1}{r_{ij}} - \frac{1}{2}\left[u^{(l)}(r_c) + \frac{2\alpha}{\sqrt{\pi}}\right] \sum_{i\in\mathcal{N}} q_i^2 \tag{19c}$$

$$= \sum_{i\in\mathcal{N}} \sum_{\substack{j\in\mathcal{N}_i - \mathcal{N}_i^{\mathrm{B}} \\ r_{ij}<r_c \\ i<j}} q_i q_j [u^{(l)}(r_{ij}) - u^{(l)}(r_c)] + \sum_{i\in\mathcal{N}} \sum_{\substack{j\in\mathcal{N}_i^{\mathrm{B}} \\ i<j}} q_i q_j \left[u^{(l)}(r_{ij}) - \frac{1}{r_{ij}}\right] - u^{(l)}(r_c) \sum_{i\in\mathcal{N}} q_i \left(\frac{q_i}{2} + \sum_{\substack{j\in\mathcal{N}_i^{\mathrm{B}} \\ i<j}} q_j\right) - \frac{\alpha}{\sqrt{\pi}} \sum_{i\in\mathcal{N}} q_i^2. \tag{19d}$$

Equation (19d) holds under a physically normal condition (i.e., state x satisfies $\|x_{ij}\| < r_c$ for every pair having a bonding interaction) and may be convenient for implementations.

The force acting on each atom i is given via the gradient of the energy, as

$$-\nabla_i E_{\mathrm{ZM}(l)}^{(\mathrm{NB})}(x) = \sum_{\substack{j\in\mathcal{N}_i \\ r_{ij}<r_c}} q_i q_j e^{(l)}(r_{ij}) \frac{x_{ij}}{r_{ij}} - \sum_{j\in\mathcal{N}_i^{\mathrm{B}}} \frac{q_i q_j}{r_{ij}^2} \frac{x_{ij}}{r_{ij}} \in \mathbb{R}^3 \tag{20a}$$

$$= \sum_{\substack{j \in \mathcal{N}_i - \mathcal{N}_i^{\mathrm{B}} \\ r_{ij} < r_{\mathrm{c}}}} q_i q_j e^{(l)}(r_{ij}) \frac{x_{ij}}{r_{ij}} + \sum_{j \in \mathcal{N}_i^{\mathrm{B}}} q_i q_j \left[e^{(l)}(r_{ij}) - \frac{1}{r_{ij}^2} \right] \frac{x_{ij}}{r_{ij}} \quad (20b)$$

for $l \geq 1$, where Eq. (20b) holds under the normal condition stated for Eq. (19d). Here,

$$e^{(l)}(r) \equiv -Du^{(l)}(r) \quad (21a)$$

$$= F(r) + \sum_{m=1}^{l} 2ma_m^{(l)} r^{2m-1} \quad (21b)$$

with

$$F(r) \equiv -DV(r) = \frac{\mathrm{erfc}(\alpha r)}{r^2} + \frac{2\alpha}{\sqrt{\pi}} \frac{\exp(-\alpha^2 r^2)}{r}. \quad (22)$$

Since $e^{(l)}(r_{ij})$ appears only as the form of $e^{(l)}(r_{ij})/r_{ij}$ in Eq. (20), in the implementation it may be convenient to use, instead of $e^{(l)}(r)$, the form of

$$f^{(l)}(r) \equiv \frac{e^{(l)}(r)}{r} = \frac{F(r)}{r} + \sum_{m=0}^{l-1} 2(m+1)a_{m+1}^{(l)} r^{2m}, \quad (23)$$

for which the polynomial is represented via even powers of distance r, likewise the pair potential function.

The first terms in Eqs. (19d) and (20b) take a usual non-bonding pairwise-sum cutoff form with utilizing the pair function $u^{(l)}(r) - u^{(l)}(r_{\mathrm{c}})$, and the second terms in these equations are the bonding pairwise-sum form utilizing $u^{(l)}(r) - 1/r$. The remaining terms in Eq. (19d) can be evaluated in advance for the simulation since it is irrelevant to configuration x. Note that if we set $\mathcal{N}_i^{\mathrm{B}}$ to be an empty set [the terms $\sum_{j \in \mathcal{N}_i^{\mathrm{B}}}$ and $\sum_{j \in \mathcal{N}_i^{\mathrm{B}}, i<j}$ vanish] for every i, then each equation in Eqs. (19) and (20) turns out to be the one for a purely non-bonded system described in Sec. II A. Thus, these equations can be seen as the equations for a general system.

III. ANALYSIS OF THE ACCURACY: PARAMETER DEPENDENCIES AND ERROR BOUNDS

The current ZM method includes three parameters, the damping parameter α [length^{-1}], cutoff length r_{c} [length], and the multipole moment l [no-dimension]. Below, we consider the unit of the length to be angstrom. After the investigation of the parameter dependence of the energy function, we analyze the error contained in the method. The error is decomposed into three kinds: replacement by the ZM summation, Eq. (5); excess energy error defined by Eq. (9), $\Delta^{(l)}$; the error via neglecting the so-called Fourier term, represented as Eq. (6) [the first term of Eq. (6b) becomes the Fourier reciprocal term in the traditional Ewald summation]. We investigate the dependence of individual errors on the parameter values, in order to obtain the knowledge how we can raise the accuracy and to analyze numerical results in detail.

A. Parameter dependence of the energy function

The energy function, Eq. (16b), is completely determined by a function

$$\mathcal{U}^{(l)} = u^{(l)} - u^{(l)}(r_{\mathrm{c}}) = V - V_l \quad (24)$$

and the constant $u^{(l)}(r_{\mathrm{c}}) + 2\alpha/\sqrt{\pi}$, which depend on α, r_{c}, and l. Figure 2(a) shows the values of $\mathcal{U}^{(l)}(r) \equiv \mathcal{U}^{(l)}(r; \alpha, r_{\mathrm{c}})$ for several values of these parameters. We see that $\mathcal{U}^{(l)}$ is decreasing function with increasing r and tends to zero at $r = r_{\mathrm{c}}$ for all the cases. Such a damping feature is far from the bare Coulombic potential and emphasized as increasing α. Also note that this damping of the potential by α is emphasized as increasing r_{c}. For example, in case of $r_{\mathrm{c}} = 8$, the value of $\mathcal{U}^{(l)}(r; \alpha, r_{\mathrm{c}})$ with $\alpha = 0.2$ is slightly smaller than that with $\alpha = 0$, while in case of $r_{\mathrm{c}} = 14$, the value of $\mathcal{U}^{(l)}(r; \alpha, r_{\mathrm{c}})$ with $\alpha = 0.2$ is one-order of the magnitude smaller than that with $\alpha = 0$. In addition, the damping is larger for a larger value of l. Namely, if we consider a larger moment l, the value of the potential function $\mathcal{U}^{(l)}$ becomes smaller. Furthermore, the difference of the value between $\mathcal{U}^{(l)}(r)$ and $\mathcal{U}^{(l+1)}(r)$ is larger, as α is small. In contrast, for a large α (e.g., $\gtrsim$0.3) the difference becomes very small (not shown) for a practical cutoff distance region. The value of $\mathcal{U}^{(l)}(r; \alpha, r_{\mathrm{c}})$ is increasing with respect to r_{c} [note the region of the horizontal axis in Fig. 2(a) is distinct for each r_{c} case].

The constant term $u^{(l)}(r_{\mathrm{c}}) + 2\alpha/\sqrt{\pi}$ shows decreasing behavior with increasing r_{c} and increasing behavior with increasing α and l [Fig. 2(b)]. These parameter dependencies are the opposite to those for the function $\mathcal{U}^{(l)}$ stated above, and such a contrast should be sought for. The difference of the constant term between l and $l+1$ is larger, as α is smaller.

Thus, combined with the similar property of $\mathcal{U}^{(l)}$, the total difference among the ZM methods with individual l values is larger as α is smaller. A small α complies with our assumption and will be used in real applications. Thus, the investigation of the difference resulting from the difference of the moment should be important, and we will also discuss this issue in numerical simulations in Sec. V. Note that the difference of the α value dependence of the energy lessens as r_{c} becomes small: regarding the pair potential, it is an alternative expression of the enhancement of the damping by α with increasing r_{c}, as stated; regarding the constant term, it means a growth of the plateau with decreasing r_{c}, as seen in Fig. 2(b).

B. Excess energy: The origin of the damping effect

In this subsection we explain the damping effect in terms of the excess energy accuracy. From Eq. (16a), the ZM energy can be represented by

$$E_{\mathrm{ZM}}^{(l)}(x) = \frac{1}{2} \sum_{i \in \mathcal{N}} \sum_{\substack{j \in \mathcal{N}_i \\ r_{ij} < r_{\mathrm{c}}}} q_i q_j [V(r_{ij}) - V_l(r_{ij})] + \mathrm{const.} \quad (25)$$

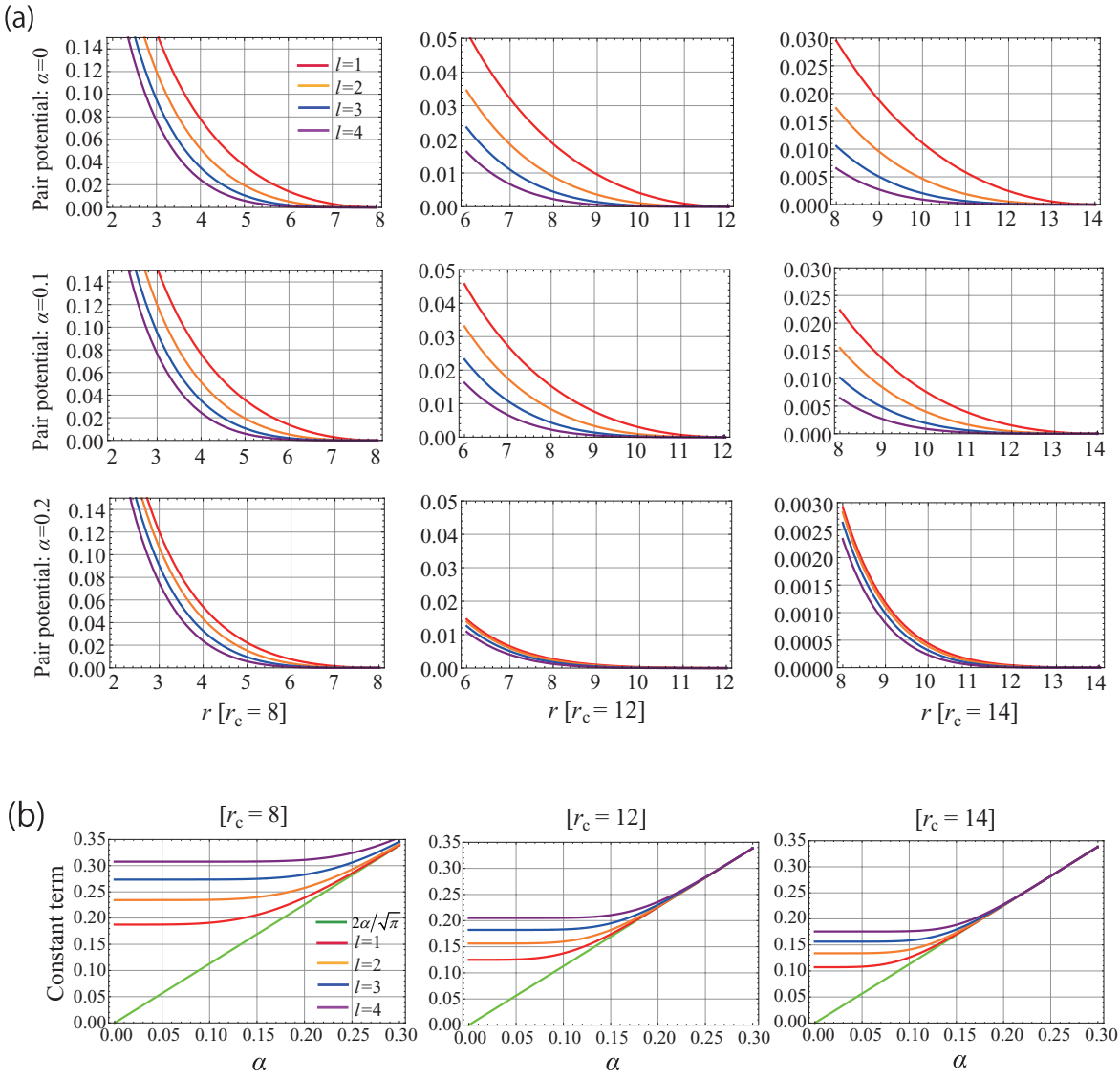

FIG. 2. (a) Pair potential functions in the ZM method with a cutoff length $r_c = 8$ Å (left), $r_c = 12$ Å (middle), and $r_c = 14$ Å (right). Top three panels show those with damping parameter $\alpha = 0$ (Å^{-1}), middle for $\alpha = 0.1$ (Å^{-1}), and bottom for $\alpha = 0.2$ (Å^{-1}). In each panel, four curves show the pair potential function with $l = 1, 2, 3, 4$, from top to bottom, respectively. Notice that the right bottom panel ($r_c = 14$, $\alpha = 0.2$) uses an enlarged vertical-axis scale, compared with the above two panels. (b) The dependence of the constant terms on damping parameter α in the ZM energy with a cutoff length $r_c = 8$ Å (left), $r_c = 12$ Å (middle), and $r_c = 14$ Å (right). In each panel, five curves show the constant terms: $2\alpha/\sqrt{\pi}$, $u^{(l)}(r_c) + 2\alpha/\sqrt{\pi}$ ($l = 1, 2, 3, 4$), from bottom to top, respectively.

While, the excess energy error is, from Eqs. (8)–(10a),

$$\Delta_{\mathrm{exc}}(x) \equiv \Delta^{(l)}(x) \tag{26a}$$

$$= \hat{E}^{(l)}(x) - \check{E}^{(l)}(x) \tag{26b}$$

$$= \frac{1}{2} \sum_{i \in \mathcal{N}} \sum_{j \in \mathcal{J}_i^{(l)}} q_i q_j [V(r_{ij}) - V_l(r_{ij})]. \tag{26c}$$

Namely, the pair potential function $V - V_l$ defining the ZM energy also describes the excess energy error defined on the excess subsets. This fact has not been clarified before even for the previous ZD scheme, and it is now clear by presenting a systematic view in considering the current ZM method.

From Sec. III A we knew the behavior of $\mathcal{U}^{(l)} = V - V_l$ with respect to the parameters including α. In fact, as increasing α, the value of $\mathcal{U}^{(l)}(r) \geq 0$ is small [Fig. 2(a)]. This indicates that if we use a large α then we can reduce the excess energy error, and this correspondence can be interpreted as the damping effect for the accuracy (by damping parameter α). On the other hand, to investigate the dependence of this error on cutoff length r_c, we should consider the following two compensating factors. First, since the members in the excess subset, $\mathcal{J}_i^{(l)}$, lie near the cutoff surface, the value of $\mathcal{U}^{(l)}(r)$ at $r \sim r_c$ comes to an issue and is decreasing with increasing r_c [Fig. 2(a)]. Second, $\mathcal{J}_i^{(l)}$ itself depends on r_c, and its extent would be, roughly speaking, proportional to r_c^2.

To consider these factors, we provide an approximated upper bound of the excess energy error. From Eq. (26), we have

$$|\Delta_{\mathrm{exc}}(x)| \leq \frac{|q|^2}{2} \sum_{i \in \mathcal{N}} \mathcal{E}_i, \tag{27a}$$

$$\mathcal{E}_i \equiv \sum_{j \in \mathcal{J}_i^{(l)}} \left| \mathcal{U}^{(l)}(r_{ij}) \right|, \tag{27b}$$

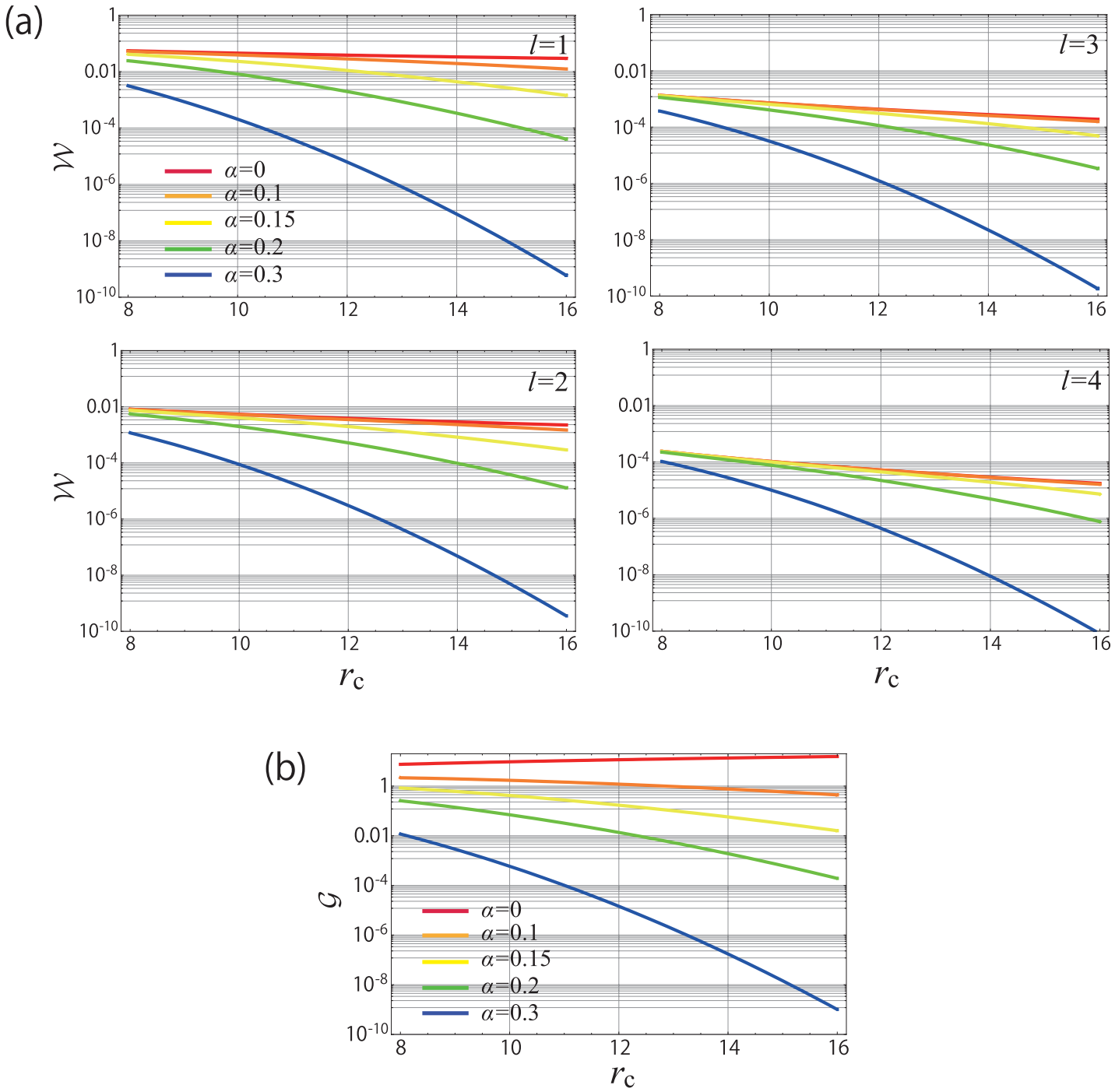

FIG. 3. (a) The factor of the upper bound of the excess energy error, Eq. (28b), for several values of the parameters: damping parameter α, cutoff length r_c, and multipole moment l. (b) The factor of the upper bound of a part of the replacement error, Eq. (32b).

where $|q| \equiv \max_{i\in\mathcal{N}} |q_i|$. As shown in Appendix B in detail, a continuous density approximation for the particle distribution leads Eq. (27) to

$$|\Delta_{\mathrm{exc}}(x)| \lesssim 2\pi N\, |q|^2\, \rho^0\, \mathcal{W}(\alpha, r_c, l, \delta), \tag{28a}$$

$$\mathcal{W}(\alpha, r_c, l, \delta) \equiv \int_{r_c-\delta}^{r_c} r^2 \left|\mathcal{U}^{(l)}(r; \alpha, r_c)\right| dr. \tag{28b}$$

Here, we have considered a spherical shell inside the cutoff sphere with width δ to mimic the space containing the particles in the excess subset $\mathcal{J}_i^{(l)}$, and ρ^0 represents an averaged number density in this shell (ρ^0 depends on r_c in general). The dependence of function $\mathcal{U}^{(l)}$ on α, r_c has been explicitly denoted.

The dependencies of $\mathcal{W}(\alpha, r_c, l, \delta)$ on parameters are shown in Fig. 3(a). We see that the value of $\mathcal{W}$ is decreasing as increasing r_c and it is also decreasing as increasing α or l. Obviously $\mathcal{W}(\alpha, r_c, l, \delta)$ is an increasing function with respect to δ (e.g., $\delta \to 0$ implies the vanishing of the excess subset), for which we set $\delta = 1$ in Fig. 3. Thus an approximated upper bound of the excess energy error is decreasing with increasing the individual values of α, r_c, and l.

Despite limitations as stated in Appendix B, the estimation of Eq. (28) is sufficient for our purpose. It is simple enough to treat the error qualitatively and is universal due to the independence of the system model. Since the absolute value of the error fluctuates between the upper bound and zero (we actually analyze the absolute error values in Sec. V), the upper bound governs the global or averaged behaviors of the absolute error, and its approximation is useful to give a rough estimation of both the error itself and the dependencies on the parameters. Thus, we shall use the most simple estimation, Eq. (28), for analyzing numerical results.

Now, the above results suggest that the excess energy error is approximately decreasing with increasing r_c or l, and also supports the consideration at the beginning of this subsection such that the excess energy error is decreasing with increasing α. Furthermore, they conform to the results of the analytic expression, Eqs. (9), (11), and (12), regarding the decreasing property for $\Delta_{\rm exc}(x)$ with respect to l. However, note that this dependence on l is wholly effective in the total accuracy if the states admit moment L [viz., the ZM condition (1) with moment L, as stated in Sec. II A] and if the theoretical moment l is smaller than or equal to the state moment L. Under this condition the total accuracy improvement with increasing l can be interpreted as the enhancement of the expressiveness of the Lth ZM state x in a given system via refining condition (1) such that it honestly describes the intrinsic neutralized subset. On the other hand, if l is larger than L, the other kind of the error may become principal, and the improvement of the excess energy error with increasing l may not become wholly effective. This error, originated from the validity of the condition $l \le L$, is classified into the replacement error, which is described below.

C. Replacement via the neutralized subset

One of the remaining two approximations concerns the replacement by the ZM summation, Eq. (5). The possible error can be represented as follows:

$$\Delta_{\rm rep}(x) \equiv \frac{1}{2}\sum_{i\in\mathcal{N}}\sum_{j\in\mathcal{N}_i} q_i q_j V(r_{ij}) - \frac{1}{2}\sum_{i\in\mathcal{N}}\sum_{j\in\mathcal{M}_i^{(l)}} q_i q_j V(r_{ij}) \tag{29a}$$

$$= \Delta_{\rm cut}(x) + \Delta_{\rm rem}(x), \tag{29b}$$

where

$$\Delta_{\rm cut}(x) \equiv \frac{1}{2}\sum_{i\in\mathcal{N}}\sum_{\substack{j\in\mathcal{N}_i \\ r_{ij}\ge r_c}} q_i q_j V(r_{ij}), \tag{30a}$$

$$\Delta_{\rm rem}(x) \equiv \frac{1}{2}\sum_{i\in\mathcal{N}}\sum_{j\in\mathcal{J}_i^{(l)}} q_i q_j V(r_{ij}). \tag{30b}$$

Equation (30a), $\Delta_{\rm cut}(x)$, is the error caused from the simple truncation of V at the cutoff length r_c. In general, as increasing r_c, this tends to be small, where it often shows oscillating and slow convergent-like behavior. In fact, as indicated in Ref. 42, the large-amplitude oscillating behavior was observed in the non-damped case. Equation (30b), $\Delta_{\rm rem}(x)$, is obtained by subtracting the neutralized sum from the simple cutoff sum. Although the quantity $\Delta_{\rm rem}(x)$ is formally classified into an "error," its signature is converse to that of $\Delta_{\rm cut}(x)$ in most cases, so it should work as a compensating (cancelling) factor to the first term.

Parameter dependency of each term can be roughly seen from the behavior of its upper bound. Since

$$|\Delta_{\rm cut}(x)| \le \frac{|q|^2}{2}\sum_{i\in\mathcal{N}}\sum_{\substack{j\in\mathcal{N}_i \\ r_{ij}\ge r_c}} V(r_{ij}), \tag{31}$$

the upper bound of $\Delta_{\rm cut}(x)$ is clearly decreasing with increasing the cutoff length r_c or the damping parameter α. For $\Delta_{\rm rem}(x)$, using a similar manner to that of the excess energy in Sec. III B, we have

$$|\Delta_{\rm rem}(x)| \lesssim 2\pi N |q|^2 \rho^0 \mathcal{G}(\alpha, r_c, \delta), \tag{32a}$$

$$\mathcal{G}(\alpha, r_c, \delta) \equiv \int_{r_c-\delta}^{r_c} r^2 V(r;\alpha) dr. \tag{32b}$$

Figure 3(b) shows that $\mathcal{G}$ is decreasing with increasing α and it is decreasing with increasing r_c except $\alpha = 0$, which becomes a special case. These results suggest that the replacement error is composed of two compensating factors and that the absolute values of the individual factor become small as r_c increases or α increases. Thus, the replacement error inclines to be small with increasing r_c or α. In particular, the replacement-error reduction with increasing α implies that the parameter α exerts the damping effect on the replacement error, as well as the excess energy error.

The dependence of $\Delta_{\rm rep}(x)$ on multipole moment l is considered through $\mathcal{J}_i^{(l)}$. In the specific case that the states are zero Lth moment states, the replacement by the ZM summation is irrelevant to l, as long as $l \le L$. This is because $\mathcal{M}_i^{(L)}$ can be used instead of $\mathcal{M}_i^{(l)}$, due to the fact that $\mathcal{M}_i^{(L)} \subset \mathcal{M}_i^{(l)}$ [see Eq. (1)] and that the resulting energy formula is irrelevant to the choice of the specificity of the neutralized subset [see Eq. (16)]. Namely, $\mathcal{J}_i^{(L)}$ can be used, instead of $\mathcal{J}_i^{(l)}$, for $l \le L$ in Eq. (30b). Since $\Delta_{\rm rem}(x)$ is thus irrelevant to l and since $\Delta_{\rm cut}(x)$ is clearly independent of l, the irrelevance of the replacement error follows. In contrast, if $l > L$, the cancellation between $\Delta_{\rm rem}(x)$ and $\Delta_{\rm cut}(x)$ would not be sufficient. Note that the validity of this assumption, viz., the most appropriate moment L exist, should be evaluated in individual cases. Our previous studies showed, for a sufficiently equilibrated, disordered system, or even for ordered crystal systems, that $l = 1$ describes the states better than $l = 0$, indicating that such systems obey $L \ge 1$. In Sec. V, we will examine these issues in specific systems.

D. Long-ranged Fourier term

The remaining approximation is neglecting the first term of Eq. (6b), $\Delta_{\rm Fou}(x) \equiv \frac{1}{2}\sum_{i,\, j\in\mathcal{N}} \frac{q_i q_j}{r_{ij}} \mathrm{erf}(\alpha r_{ij})$. Obviously this

is irrelevant to r_c and l. From the fact that

$$|\Delta_{\mathrm{Fou}}(x)| \leq \frac{|q|^2}{2} \sum_{i\in\mathcal{N}} \sum_{j\in\mathcal{N}} \frac{\mathrm{erf}(\alpha r_{ij})}{r_{ij}} \tag{33}$$

and from the increasing feature of $\mathrm{erf}(\alpha r)$ with increasing α, this kind of error would become large as α increases. Thus, the existence of this error becomes the compensating factors to the damping effect, which is demonstrated for both the excess energy error and the replacement error. The damping effect will become negligible by increasing the cutoff length, which will be discussed again in Sec. V. On the other hand, $\Delta_{\mathrm{Fou}}(x)$ decreases with small α values, and it completely vanishes when we use $\alpha = 0$.[73,74] Note that more specific analyses for this kind of the error were done in detail in Ref. 42.

E. Summary with remarks

An upper bound (not necessarily the supremum) of each of the three kinds of the energy error was discussed. The error bounds should govern the global behavior of individual errors. For $\Delta_{\mathrm{exc}}(x)$ and $\Delta_{\mathrm{rem}}(x)$, we have assumed the continuity and isotropy regarding the excess subset, which are plausible for bulk liquids and should be useful to study liquid systems in Secs. IV and V.

The parameter dependencies of the estimated upper bounds of the individual errors are shown in Table I. Here we assume $l \leq L$ with L being the moment of the system. Characteristic features are as follows:

(i) The behavior of the excess energy error and that of the replacement error are similar, but is different with respect to the l dependence.
(ii) For the dependence on r_c, we see that each error is decreasing or irrelevant. This cooperative (non compensational) feature also applies to the dependence on l. Only α generates the compensations, i.e., decreasing with respect to both the excess energy error and the replacement error (these properties form the damping effect) but increasing with respect to the Fourier term error.

The error analysis of the energy based on the formula, Eq. (16), discussed thus far is for non-bonded systems, but it also applies for general molecular systems. This is because the energy formula, Eq. (19), for the latter systems differs from that of the former systems only in the second term of Eq. (19b) or that of Eq. (19c), which can be exactly evaluated. This is essentially the same for Eq. (19d), which was used in our numerical investigations.

TABLE I. Parameter dependencies of the upper bounds of the individual three kinds of the energy errors in the ZM method: the replacement error ("Rep."), the excess-energy error ("Exc."), and the Fourier-term error ("Fou."). The parameters are the cutoff length r_c, the damping parameter α, and the multipole moment l. For example, for the column of parameter r_c, the upper bound of Rep. is *decreasing* with increasing r_c, that of Exc. is *decreasing* with increasing r_c, and that of Fou. is *irrelevant* to r_c. The dependency of each upper bound leads to a rough estimation of the dependency of the corresponding energy error on the parameters.

Error	r_c	α	l
Rep.	Decreasing[a]	Decreasing	Irrelevant[b]
Exc.	Decreasing[a]	Decreasing	Decreasing
Fou.	Irrelevant	Increasing	Irrelevant

[a]It does not necessarily mean a monotonic decreasing, due to the reflection of the structure factor.
[b]We assume $l \leq L$ with L being the moment of the system.

IV. SIMULATION METHOD

The specific performance of the current method is discussed via numerical investigations by MD simulations on a NaCl liquid system and a bulk liquid water system.

A. NaCl

We examined a three-dimensional bulk NaCl system composed of 2304 ions (pure ion system including no other material such as water molecules) obeying the Born–Mayer–Huggins (BMH) potential.[78] After an equilibration run with the isotropic *NTP* (constant temperature and pressure) MD simulation at temperature of 1100 K and pressure of $P = 1$ atm, which correspond to a liquid phase, we started two kinds of MD simulations via the myPresto program.[79]

The first one was a 1 ns NTV (constant temperature) simulation at temperature of 1100 K, using the smooth particle mesh Ewald (PME) method[80] for calculating the electrostatic interactions. This was done to sample the particle configurations for investigating the accuracy of the ZM methods. The energy error at the obtained configuration x was estimated through the difference between the current Coulombic energy $E_{\mathrm{ZM}}^{(l)}(x)$ and the reference Coulombic energy $E(x)$, which was evaluated by the Ewald method,[4] and we averaged the error ratio over $n_x = 1000$ configurations, as

$$\Delta_{\mathrm{ZM}(l)} \equiv \frac{1}{n_x} \sum_x \left| E_{\mathrm{ZM}}^{(l)}(x) - E(x) \right| / |E(x)|. \tag{34}$$

For the multipole moment, we used $l = 2, 3, 4$, which correspond to the methods for the zero-quadrupole, zero-octupole, and zero-hexadecapole, respectively. We also used $l = 1$, which corresponds to the ZD method. In both the Ewald and PME methods, the damping parameter was 0.35 $\mathrm{Å}^{-1}$ and the cutoff length of the real part evaluation was 12 Å.

Another kind of simulation was a 1 ns NVE (constant energy) simulation using the ZM method for calculating the electrostatic interactions. This was done to investigate the stabilities of the MD simulations with employing the ZM method, using the standard velocity Verlet integrator with the time step of 2 fs. We investigated the total-energy conservations regarding the ZM methods with $l = 1, 2, 3, 4$ and $\alpha = 0.1$ and 0 $\mathrm{Å}^{-1}$. Initial temperatures for all the cases were set to be 1100 K. Cutoff length was 12 Å for the BMH potential energy including the Coulombic energy, and a simple straight truncation was used for the attractive and repulsive terms of the BMH function except the Coulombic term.

B. Water

A bulk water system of 4178 molecules of a simple TIP3P model[81] was studied. Similar to the NaCl case, an

equilibration MD run under the isotropic *NTP* ensemble with the temperature of $T = 300$ K and the pressure of $P = 1$ atm was preliminary, and two kinds of MD simulations were performed.

The first one was a 2 ns NTV MD simulation with employing the PME method ($\alpha = 0.35$ Å^{-1}, $r_c = 12$ Å) at $T = 300$ K to sample the configurations for investigating the accuracy of the current ZM method. The energy accuracy was evaluated by

$$\Delta^{(\mathrm{NB})}_{\mathrm{ZM}(l)} \equiv \frac{1}{n_x} \sum_x \left| E^{(\mathrm{NB})}_{\mathrm{ZM}(l)}(x) - E^{(\mathrm{NB})}(x) \right| / |E^{(\mathrm{NB})}(x)|, \quad (35)$$

using Eq. (19d) for the ZM methods with multipole moments $l = 1, 2$ and using Eq. (18b) for the reference energy evaluated by the Ewald method. Here, $n_x = 1000$ configurations were sampled at every 1 ps during the last 1 ns.

The second one was a 2 ns NTV MD simulation at $T = 300$ K using the ZM method with $l = 2$ to calculate the radial distribution function (RDF) as a structural property of this water system. The parameters were $\alpha = 0.06$ Å^{-1} and $r_c = 12$ Å. The RDF, $g_{\mathrm{ZM}}(r)$, with respect to the distance, r, of two oxygen atoms were evaluated. With the same protocol, we calculated the RDF using the PME method ($\alpha = 0.35$ Å^{-1}, $r_c = 12$ Å), $g_{\mathrm{PME}}(r)$, and measured the discrepancies between the methods via a ratio, $\Delta g_{\mathrm{ZM}}(r) \equiv |g_{\mathrm{ZM}}(r) - g_{\mathrm{PME}}(r)| \,/\, |g_{\mathrm{PME}}(r)|$. For comparison, we also calculated similarly the RDF by a MD simulation using the force-switching (FSw-)Wolf ZC method[70] with parameters $\alpha = 0.14$ Å^{-1} and $r_c = 12$ Å [$g_{\mathrm{ZC}}(r)$], and that using the ZD method[72] with $\alpha = 0.06$ Å^{-1} and $r_c = 12$ Å [$g_{\mathrm{ZD}}(r)$], where these parameters showed good efficiencies in the previous studies.[73] Discrepancies between these methods and the PME method were also measured similarly via $\Delta g_{\mathrm{ZC}}(r)$ and $\Delta g_{\mathrm{ZD}}(r)$, respectively.

The SHAKE algorithm was used to maintain the shape of the TIP3P molecule. We used the atom-based cutoff mode with $r_c = 12$ Å for both the electrostatic and vdW interactions. The importance of the atom-based mode was discussed in Refs. 13 and 73.

V. RESULTS AND DISCUSSIONS

A. NaCl liquid

1. Energy accuracy

Figure 4 shows the electrostatic energy errors calculated by the ZM summation methods with several values of the damping parameter α, cutoff length r_c, and moment l. Although associated with oscillations, the errors were lower on average for a larger cutoff length, and sufficient accuracies were attained at practical cutoff distances, e.g., 11–16 Å. For example, the error for $\alpha = 0.14$ was sufficiently small (0.023%) at a short cutoff length of $r_c = 11$ Å under the moment of $l = 2$; while for $l = 3$, the error with no-damping case ($\alpha = 0$) is ∼0.008% at $r_c = 12.5$ Å. Apart from the detailed differences provided by the difference of the value of the parameters, we see that the accuracy is better for a larger value of moment l up to $l \lesssim 3$, on average. The errors for $l = 1$ are less than 0.1% if we take $r_c > 13$ Å, those for

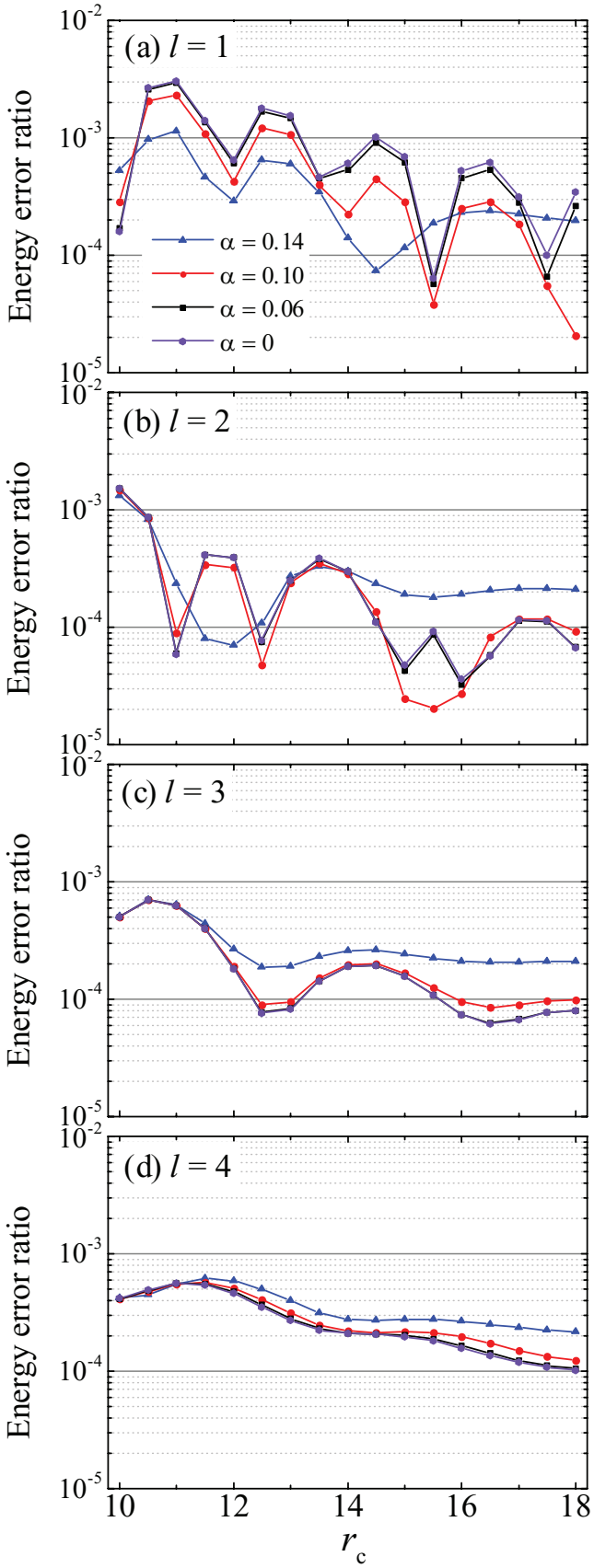

FIG. 4. The error ratio of the electrostatic energy of the ZM summation method, $\Delta_{\mathrm{ZM}(l)}$ [Eq. (34)], using the reference energy obtained by the Ewald method, in the molten NaCl ion system. $l = 1$ corresponds to the ZD method; $l = 2, 3, 4$ corresponds to the current method for the zero-quadrupole, zero-octupole, and zero-hexadecapole, respectively. The parameter r_c (Å) indicates the cutoff length and α (Å^{-1}) the damping parameter.

$l = 2$ attain this accuracy at $r_c > 10$ Å, and those for $l = 3$, 4 attains this for all r_c values we simulated. Although the oscillations are reduced, the error for $l = 4$, compared with that for $l = 3$, seems to be similar, or larger at certain r_c regions according to the oscillating behavior for $l = 3$. This should be due to that many states $\{x\}$ were the states described well with the third moment, as will be demonstrated below in detail.

In what follows, the dependence of the error on the values of parameters will be analyzed in detail. At first glance, the behavior of the energy error curve for, e.g., $l = 2$, seems to be complicated and peculiar, compared with those for other ls. Including this issue, in order to understand the total behaviors, we analyze them with two specific viewpoints, *crossing* and *oscillation*, of the error curves. These viewpoints, as well as the theoretical analyses discussed in Sec. III, enable us to provide a unified interpretation of the parameter dependencies of the error.

a. Error curve crossing. For a small l, typically as seen in the case of $l = 1$ in Fig. 4, larger the value of α, the energy error is smaller. In fact, the damping effect in the ZC method is important to attain the high accuracy.[42,72,73] However, this feature does not necessarily hold for a higher l. In fact, for $l = 3, 4$, totally opposite behavior is observed: the energy error is smaller as the value of α is small. While, for a mid range of l, viz., $l = 2$, a mixed behavior, i.e., crossing between the error curves with different α values, is observed: the energy error for a larger value of α is smaller at a small r_c and the error for a smaller value of α is smaller at a large r_c. Such crossings are explicitly observed, e.g., for $l = 2$ at a cutoff length $r_c \cong 13$ Å among $\alpha = 0.14$ and $\alpha < 0.14$, and also for $l = 1$ at $r_c \cong 15$ Å between $\alpha = 0.14$ and 0.1. In fact, these crossings should not simply be the "mixed" behavior, but will lead to a unified picture. Namely, the crossing will occur for all l, but it will be observed at a very large r_c for a small l and observed at a very small r_c for a large l ($\gtrsim$3). The phenomena of the crossing itself is originated from the dependency of the accuracy of the method on parameters α and r_c, and it is affected by the moment l. The reason for the crossing and its dependence on l will be clarified below, which is also important to attain the efficiency via an appropriate choice of the parameter values.

The reason why the crossing between the curves with different α values occurs at each moment l is due to two factors. As discussed in Secs. III B and III C, the replacement error $\Delta_{rep}(x)$ and the excess energy error $\Delta_{exc}(x)$ are smaller for a larger r_c. In addition, as α increases, these errors are smaller, which is interpreted as the damping effect. On the basis of these findings, first, imagine two energy error curves that reflect *only* $\Delta_{rep}(x)$ and $\Delta_{exc}(x)$ [viz., not involve $\Delta_{Fou}(x)$], where the one curve is with a small α and the other with a large α. Then, the curve with a large α is positioned under the curve with a small α, in most region of r_c. This is due to the damping effect and the finding in Sec. III A such that the α-value dependence of the energy function, and thus that of the error, lessen as r_c becomes small. Second, consider the remaining factor, $\Delta_{Fou}(x)$, which is due to ignoring the Fourier term. This error is larger as α is larger, and it is irrelevant to r_c (Sec. III D), so remaining even at an arbitrary large r_c, in contrast to $\Delta_{rep}(x)$ and $\Delta_{exc}(x)$. Now, when we add the contribution of $\Delta_{Fou}(x)$ into the individual two curves considered above (viz., all the errors are included), the curve with a large α is shifted upward with a larger amount, compared with that with a small α. At the same time we should aware that the curves are bounded from below, since they represent the absolute values of the error. Thus crossing occurs even in a moderate r_c region. Namely, the difference of the parameter dependencies between $\Delta_{rep}(x) + \Delta_{exc}(x)$ and $\Delta_{Fou}(x)$ brings the observed error-curve crossing.

We then consider the reason for the faster crossing (viz., the crossing at a smaller r_c) observed in a larger moment l, under the assumption that many states are zero Lth moment states, where $L \sim 3$ in the current case. First, we shall state that the energy accuracy is higher as increasing l until $l \leq L$. From the discussion in Sec. III, we see that the error relevant to moment l is only the excess energy, and the other two errors are almost irrelevant to l as long as $l \leq L$, under the above assumption. We also see that the degree of the approximation of the excess energy is higher as l becomes larger. This is the reason why the total accuracy is superior as l ($\leq L$) increases. Second, we shall point out that this energy accuracy refinement with respect to increasing l should be better for a smaller value of α. To explain this feature, we note that the energy difference between l and $l + 1$ is larger as α value decreases. As stated in Sec. III A, this can be clearly confirmed by the difference of the pair potential function and the difference of the constant term in the energy expression, where both differences are larger as the value of α decreases. Therefore, the accuracy of the energy with $l + 1$ should be higher than that with l as α becomes small (as long as $l + 1 \leq L$). This explains the reason for the faster crossing for a higher moment l. Namely, imagine the curves with α_S and that with α_L, for which $\alpha_S < \alpha_L$ and the both of them are obtained by using the same moment l, and imagine that they are crossing, viz., the curve with α_S is above that with α_L for a small r_c and vice versa for a large r_c. Also imagine other two curves having α_S and α_L, respectively, but having moment $l + 1$. Then, from the above reason, the curve with α_S and $l + 1$ should be positioned *greatly* lower compared with the curve with α_S and l, since α_S is relatively small; in contrast, the curve with α_L and $l + 1$ be *slightly* lower compared with the curve with α_L and l, since α_L is relatively large. Therefore, the cutoff length r_c at which the crossing occurs becomes smaller for $l + 1$, compared with that for l. This is the reason of the fast crossing for a larger moment l.

b. Oscillation. We observe the oscillations in energy error curves with respect to a cutoff length. We see that this phenomena is relevant to the method for calculating the electrostatic interaction (viz., it depends on the value of the multipole moment l, implying distinctive method), and we will see in Sec. IV B that this phenomena is also relevant to the physical system.

We first consider the origin of the oscillation. We note that the system should have a certain configurational structure, which is typically represented by the RDF. In Fig. 5 we

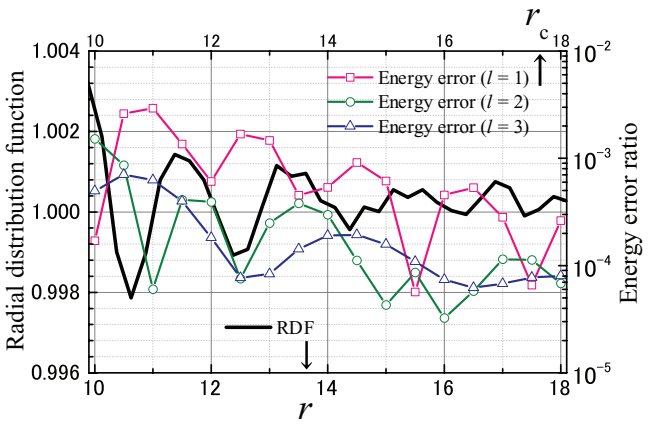

FIG. 5. Radial distribution function [horizontal axis shows the distance of two oxygen atoms, r (Å)] obtained by the PME method, and the energy errors [horizontal axis shows the cutoff radius r_c (Å)] obtained by the ZM method [α (Å^{-1}) = 0.06] with moment $l = 1, 2, 3$, in the molten NaCl ion system.

exhibit the RDF in a tail region, 10 Å $\leq r \leq$ 18 Å, obtained by the PME method, and observe the oscillations with the period of about 1–2 Å. In fact, in the strongly-coupled regime (corresponding to the melt), a single radial charge-distribution function is oscillating[82,83] with respect to distance r between two ions, and the oscillation in this function concerns with the difference between the two ion sizes, the bare-ionic-strength parameter (the charge value, the ion density, and the temperature), and the boundary conditions. In Fig. 5 we also exhibit the energy errors of the ZM methods with $l = 1, 2, 3$ using a typical parameter value, i.e., $\alpha = 0.06$. This implies a coherence or relevance between the energy error oscillations and the RDF oscillation. We try to explain this issue by using the error analyses in Sec. III. Suppose simply an isotropic situation and consider a certain cutoff sphere of an arbitrarily fixed particle. When we choose the value of the cutoff length r_c to be near the distance at which the particle density, ρ^0, is high, the number of the members in the excess subset $\mathcal{J}_i^{(l)}$ becomes relatively large, since such a member should be near the surface. Thus, as well as Eq. (26), Eq. (28a) suggests that the excess energy error $\Delta_{\rm exc}(x)$ becomes large at this cutoff length, and this mechanism would induce the error oscillation. Similar discussion also applies to the term $\Delta_{\rm rem}(x)$ in the replacement error, as seen from Eq. (32a). Likewise, for $\Delta_{\rm cut}(x)$ [Eq. (30a)], its value tends to be large near this cutoff length, although a certain phase shift between $\Delta_{\rm exc}(x) + \Delta_{\rm rem}(x)$ and $\Delta_{\rm cut}(x)$ should be considered since $\Delta_{\rm cut}(x)$ concerns the outside of the cutoff surface and $\Delta_{\rm exc}(x) + \Delta_{\rm rem}(x)$ concerns the inside of the cutoff surface. The remaining error, $\Delta_{\rm Fou}(x)$, is irrelevant to this issue, since this error does not concern with the choice of the value of r_c. Note that a slightly more analytic explanation is possible regarding the excess energy error. That is, due to the enlargement of $\mathcal{J}_i^{(l)}$ stated above, the number of the nonzero components of initial displacement vector $h_0^{(i)}$ increases, which enlarges $\|h_0^{(i)}\|$. Thus, the excess energy error $\Delta_{\rm exc}(x) = \Delta^{(l)}(x)$, described by Eqs. (9), (11), and (12), inclines to be large.

We can proceed to explain the fact that the amplitude of the oscillation is smaller as increasing the value of moment l. In Sec. III, we have seen that the error component that is strongly relevant to moment l is only the excess energy error, and that the excess energy error has a decreasing tendency with increasing a moment l. Thus, if we raise the value of l then the accuracy of the excess energy with choosing r_c at which the member density of $\mathcal{J}_i^{(l)}$ is high should be principally improved. In fact, if we suppose that $\rho^0 \equiv \rho^0(r_c)$ is oscillating with respect to r_c in Eq. (28a) [or else, density $\rho_i^{(\beta)}(r)$ in Eq. (B2) is oscillating with respect to r], then the oscillation of $\Delta_{\rm exc}(x)$ would be originated from that of $\rho^0(r_c)$, and the amplitude of the $\Delta_{\rm exc}(x)$ oscillation should be more suppressed as increasing l because $\mathcal{W}$ is decreasing with increasing l (as seen in Fig. 3(a)).

Nevertheless, we should point out that the above consideration that connects with the structural feature and the energy accuracy is still incomplete. In fact, we should explain the relations of, not only the period and amplitude of the oscillation, but also the phase of the oscillation, between the error and the RDF. The phase shift between $\Delta_{\rm cut}(x)$ and $\Delta_{\rm exc}(x) + \Delta_{\rm rem}(x)$ has been stated above, and the value of this shift is allowed to depend on moment l, since the latter, especially $\Delta_{\rm exc}(x)$, depends on l [$\mathcal{U}^{(l)}(r)$ is used in $\Delta_{\rm exc}(x)$ but $V(r)$ is used in $\Delta_{\rm rem}(x)$]. This may be the origin of the observed phase-difference on l, while more explicit discussions will be required. Regarding the charge cancellation, it would give a finer conclusion by considering the radial *charge* distribution function, rather than just the RDF. However, in any case, the behavior of the oscillation and its dependence on the method—a multipole moment—, especially for the amplitude, were evidenced in numerical simulations for the first time.

2. Stability

Conservation of the total energy (total potential energy plus the total kinetic energy) in NVE MD simulation with the ZM method was studied to investigate the stability in integrating the MD equations of motion. We set the cutoff length of $r_c = 12$ Å, which is in a practical region, and damping parameter of $\alpha = 0.1$ Å^{-1}, which showed an average behavior in the energy errors (Fig. 4). As seen from Fig. 6, the conservations were good enough for these damped cases using $\alpha = 0.1$, in spite of the fact that the BMH potential, except the Coulombic terms, was straight cut off at the same cutoff distance. In fact, the standard deviations of the trajectories were 0.183, 0.139, 0.135, 0.135 kcal/mol for the ZM methods with the moment $l = 1, 2, 3, 4$, respectively. For a larger l, the pair potential function is more damped near the cutoff distance [see Fig. 2(a)], which fact leads to the stability and conforms with these simulation results. Another reason of the relatively large deviation in the case of the lowest moment, $l = 1$, might be due to the average temperature of the system, which were almost 1100 K (liquid phase) for $l = 2, 3, 4$, and eventually 1130 K for $l = 1$. The non-damped cases, viz., using $\alpha = 0$, also showed similar behaviors and sufficient conservations for all these l values (not shown). Their standard deviations were 0.188, 0.137, 0.137, 0.134 kcal/mol for $l = 1, 2, 3, 4$, respectively. Although the damping strength of the function becomes weaker as decreasing α [Fig. 2(a)], the results of the minimum value, $\alpha = 0$, gave the similar stability

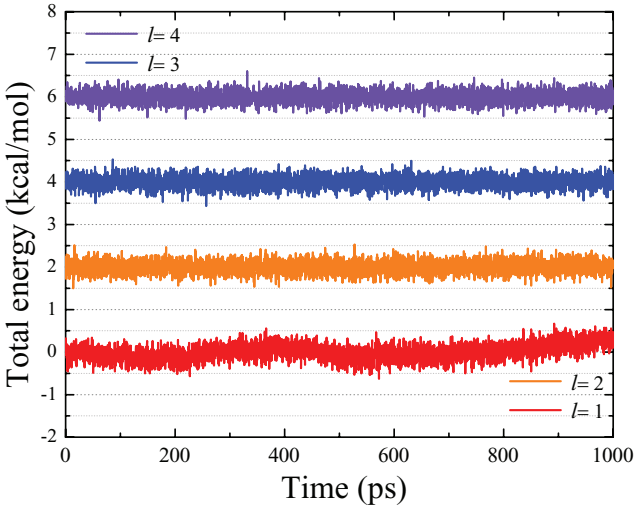

FIG. 6. Total-energy trajectories of the NVE MD simulation for the molten NaCl ion system, using the velocity-Verlet integrator with a 2 fs timestep. The electrostatic interaction was calculated by the ZM summation method with $l = 1, 2, 3, 4$ (from bottom to top), using the cutoff length of $r_c = 12$ Å and the damping parameter value of α (Å^{-1}) $= 0.1$. The vertical axis shows the difference (kcal/mol) of the total energy between the instantaneous value and the time-averaged value, where the individual trajectories are shifted with 2 kcal/mol for every moment l for clarity.

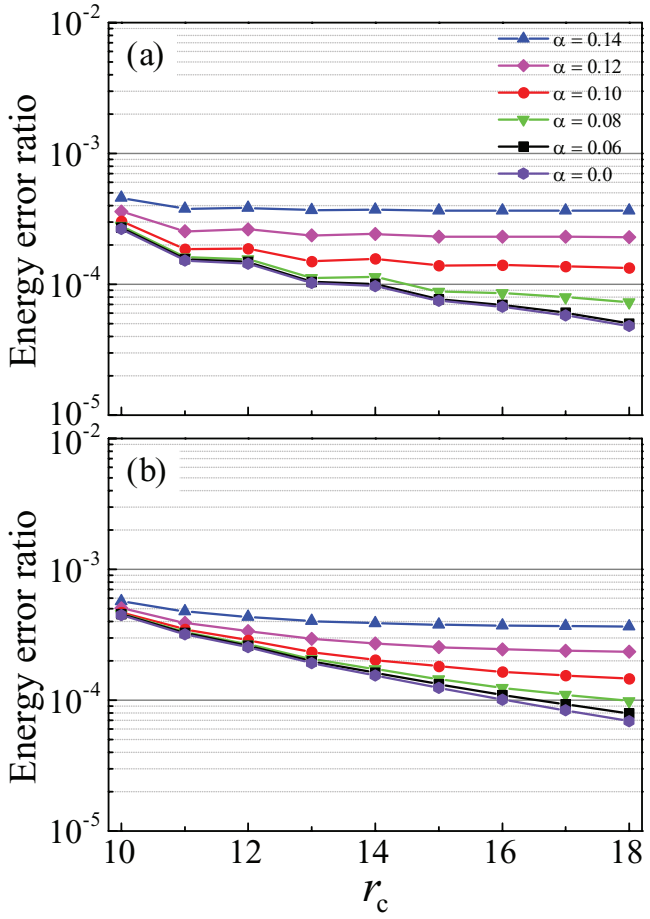

FIG. 7. The error ratio of the electrostatic energy for the ZM summation method, $\Delta^{(\mathrm{NB})}_{\mathrm{ZM}(l)}$ [Eq. (35)], using the reference energy obtained by the Ewald method, in the TIP3P bulk water system. (a) shows the errors of the ZM summation method of moment $l = 1$ and (b) that of $l = 2$. The parameters r_c (Å) and α (Å^{-1}) indicate the cutoff length and the damping parameter, respectively.

with those of $\alpha = 0.1$. This means that the pair potential function is well designed to ensure the stability in integrating the equations.

In principle, these energy conservations are yielded by a sufficient smoothness of the potential function. However, this is not necessarily trivial,[84,85] as seen in the fast multipole method,[58] which utilizes the hierarchy of meshes to approximate the particle positions. In addition to the smoothness, an atom-based cutoff mode[86] is also critical in the CB method,[73] and a pairwise expression of the potential energy is yet useful. In fact, these three issues also ensure the conservation of the total momentum P and the conservation of the center of mass when $P = 0$ initially, typically in NVE simulations. These conservations are yielded by the vanishing of the total force, and it is indeed zero in the ZM method. The pairwise expression is not only simple but important to lead to this vanishing, since it ensures the translational invariance of the potential energy function. This kind of stability is also not necessarily trivial,[87] as seen in the PME method, which utilizes the grid to capture the function.

B. Bulk water

1. Energy accuracy

Regarding the water system, Fig. 7 shows the results of the energy errors for the ZM methods utilizing the scheme described in Sec. II B. Similar to the NaCl case, the errors decreased with increasing cutoff distance r_c and became sufficiently small in a practical distance region. In addition, the error curves of the ZM method with $l = 2$ are smoother than those with $l = 1$.

However, we should point out three points that are distinguishable from the NaCl case. The first one is the α dependence: as α is smaller, the errors are smaller, in a practical r_c range shown in Fig. 7. Although this seems to be totally different from that of the NaCl system, this is not the qualitative difference but a quantitative difference. Namely, in contrast to the NaCl system, as discussed in Ref. 73, the error crossings in the water system occurs at a smaller r_c less than 10 Å (out of the practical range), and in a practical cutoff range we just observe the behavior *after* the crossing. This fast crossing is due to the fast convergence attained in the water system. Such a fast convergence can be accounted for by the randomness or mobility provided by the water molecule system, for which the randomness must supply a more flexible configurational combination so as to enlarge a neutralized subset, viz., reduce an excess subset $\mathcal{J}_i^{(l)}$, relative to the cutoff sphere. Then $\Delta_{\mathrm{exc}}(x)$ and $\Delta_{\mathrm{rem}}(x)$ should become small. On the other hand, for small α values, we assume that global quantities $\Delta_{\mathrm{cut}}(x)$ and $\Delta_{\mathrm{Fou}}(x)$ are almost unchanged, or consider that the α dependencies of these two quantities are almost unchanged. Thus the total error tends to be small, especially for a small r_c, but the tendency is suppressed for a

large r_c, since the convergent value is similar due to the remaining of $\Delta_{\mathrm{Fou}}(x)$. This mechanism would induce the fast convergence, resulting in the fast crossing of the error curves. Regarding the effect of reducing $\mathcal{J}_i^{(l)}$, relatively small sizes of the atomic radii in individual water molecules (the vdW radius of the hydrogen and that of the oxygen), compared with that in the ion system (the ionic radius of chlorine is especially large), may also contribute, since a small radius of j results in small $\|h^{(i)}_{0,\,j}\|$ for each $j \in \mathcal{J}_i^{(l)}$ [or it corresponds to lessen δ in $\mathcal{W}(\alpha, r_c, l, \delta)$ in Eq. (28b)].

The second distinguishable point is that the oscillation amplitude is very small compared with the NaCl case. One possible reason is that a prominent characteristic structure does not appear in a radial direction with a far distance in the water system (e.g., at the distance larger than 12 Å; see also Sec. V B 2), in contrast to the NaCl liquid system. Another possible reason is that the oscillation, which should be originated from the enlargement of $\Delta_{\mathrm{exc}}(x)$, $\Delta_{\mathrm{rem}}(x)$, and $\Delta_{\mathrm{cut}}(x)$ as stated in Sec. V A 1 b, is diminished by the decrease of $\Delta_{\mathrm{exc}}(x)$ and $\Delta_{\mathrm{rem}}(x)$ in the water system, where these two errors are defined on $\mathcal{J}_i^{(l)}$ and the reduction of $\mathcal{J}_i^{(l)}$ has been suggested from the two mechanisms discussed above.

The third point is that the energy accuracy for a higher moment method, $l = 2$ in the current case, is similar or slightly lower (for small α and r_c) than that for $l = 1$ in the water system. This can be understood that the zero-quadrupole (or a more higher) moment assumption is not necessarily suitable in the water case, in contrast to the NaCl case. On the basis of this observation and the fact that the accuracy for $l = 1$ is superior than that for $l = 0$,[73] the description with the zero dipole seems to be the most appropriate in the current water system, viz., $L \sim 1$.

Recall that the explanations so far to interpret the numerical results obtained by the ZM scheme require the assumption, $l \le L$, in most cases. Namely, the moment l of the utilized method should be less than or equal to L, where sufficiently many states in concern are assumed to be well described by the zero Lth moment. For example, the interpretation of the faster crossing behavior of the error curves for a higher moment observed in the NaCl case cannot be applied to the current water case. In fact, such a behavior was not observed in the water system if we compare the results between $l = 1$ and $l = 2$. However, the interpretation applies to $l = 0$ and $l = 1$, since they are $\le L$, and in fact the faster crossings in $l = 1$ than that in $l = 0$ were observed.[73]

Finally we note that these results do not necessarily mean that the ZM scheme with $l = 2$ is inferior to that with $l = 1$. This is because the values of the energy error themselves in the scheme with $l = 2$ are sufficiently small to be acceptable. In addition, the static property was fairly well described in the scheme with $l = 2$ than those with $l < 2$, as discussed below.

2. Static property: RDF

Figure 8 shows the RDFs of the water system, obtained by the PME method and by the ZM method with $l = 1$ and $l = 2$. For comparison, we show the results of the FSw-Wolf ZC method, which was used to stably conduct the MD simulation with the method corresponding to the $l = 0$ scheme[70] (note the FSw-Wolf method is not equivalent to the $l = 0$ ZM scheme but accommodates to it). As seen in the inset, overall the distance range, the structures obtained by the PME method are captured by the ZM methods. Here, we concentrated on the tail region of the RDFs as emphasized in the figure, because the previous study[73] reveals that the differences from the PME remain near the cutoff length in the ZD method (i.e., the $l = 1$ case).[8] In fact, although better than the ZC scheme, the error in the ZD method is oscillating around the cutoff length of $r_c = 12$ Å with the maximum amplitude of about 2%. In contrast, the error in the ZM method with $l = 2$ was smaller by nearly one-order of magnitude than that with $l = 1$ (the differences of the solid curves between the $l = 2$ ZM and the PME are invisible in the figure).

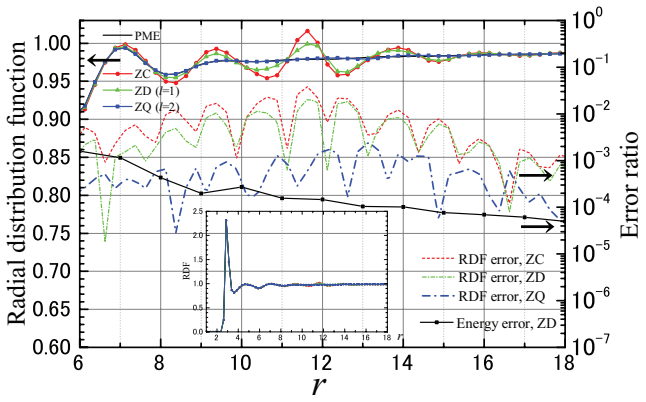

FIG. 8. RDFs (no dimension) with respect to the distance of two oxygen atoms, r (Å), for the TIP3P water molecule system, obtained by the PME method, the FSw-Wolf ZC method, the ZD method (ZM method with $l = 1$), and the ZQ method (ZM method with $l = 2$). The cutoff lengths were $r_c = 12$ Å for all the methods. The top four curves show the values of RDFs (left vertical axis) by the individual methods (ZQ and PME overlap). The inset shows the RDFs in a whole distance region. Three dashed curves show the discrepancies (the right vertical axis) from the PME, viz., the ratios Δg_{ZC}, Δg_{ZD}, and Δg_{ZM}. For comparison, the energy error ratios of the ZD method [α (Å^{-1}) = 0.06] (as in Fig. 7) are also indicated (right vertical axis), where the horizontal axis should be read as the cutoff length (Å).

This improved accuracy would be a consequence of the increased smoothness of the $l = 2$ scheme potential function, compared with the $l = 1$ scheme potential function, especially at the vicinity of the cutoff distance. In fact, moment l induces a scheme of class C^l.[77] Alternatively, a large α or a large r_c has a similar smoothing effect,[73] so that such a parameter choice was effective to attain the smaller discrepancy in the RDF. We here find that a more drastic improvement can be obtained by simply using a higher l.

One can observe that the oscillations of the energy error curves, where the result obtained by the method with $l = 1$ is shown as a typical case in Fig. 8, seem to be coherent to the behavior of the RDF. As was done in the NaCl study in Sec. V A 1 b, this feature should explain the energy error oscillation. However, compared with the NaCl case, the oscillations in the RDF (obtained by the PME) with the distance range 10 Å $\lesssim r \lesssim$ 18 Å is small in the water case, and this should explain the small energy error oscillations observed in the ZM method with $l = 1$ and $l = 2$ in the range of 10 Å $\le r_c \le$ 18 Å.

VI. CONCLUSIONS

We have investigated the zero-multipole summation method, which was developed for evaluating the electrostatic energy of a point charge particle system in molecular simulation. The current study reveals the properties of the method by numerical simulations of the TIP3P bulk water system and the molten ion system with the BMH force field, with the aid of theoretical error analyses. We investigated the parameter dependencies of the ZM energy function and analyzed the error of the method theoretically and numerically.

Utilizing a positive damping parameter α in the pair potential function is effective in many cases to raise the accuracy of the cutoff-based method, as is known in the studies of the ZC Wolf method. We revealed the origin of the damping effect from the viewpoint of the excess energy error and the replacement error. We found that the excess energy error can be expressed by the evaluation of the pair potential function itself on the excess subset. Such a theoretical interpretation was done for the first time, to the best of our knowledge. We provided an approximated upper bound of the excess energy error and found that it is decreasing with increasing the values of α, r_c, and l. Such parameter dependencies were investigated also for both the replacement error and the Fourier term error. These theoretical estimations are useful to understand various phenomena obtained by the numerical simulations, to seek a better assignment of the parameter values, and to promote the further development of the method.

In the numerical simulations of the NaCl liquid system, sufficient accuracies were obtained in a practical cutoff distance region. We confirmed that the energy accuracy can be improved by raising the multipole moment l, up to $l = 3$. We investigated the characteristic phenomena of the crossing of the energy-error curves with individual α values, and analyzed the features and the origin. The origin is the compensation between the damping effect and the anti-effect of ignoring the Fourier term. This can be simply understood from the dependencies of the three-kind errors on α and r_c. The reason that the crossing is faster with increasing the moment can be explained by the two factors: one is the accuracy improvement of the excess energy by increasing l; another one is the enhancement of the degree of the total accuracy improvement within $l \leq L$ as the value of α is small.

We have analyzed the energy error oscillation with respect to the cutoff length. We found its origin to be relevant to the structure of the system such that the excess energy error and the replacement error become large when we set the cutoff length near the distance at which the particle density is high. The reasons why the oscillation amplitude is low for a larger moment l should be due to the improvement of the excess energy accuracy as increasing l. However, for a complete understanding, we have to explain the origin of the phase shift for a certain l, although we have pointed out a possible reason generated from the difference in the features among individual error terms. In addition, for a better grasp of the coherence between the energy error oscillations and the structural property of the system, further investigations such as varying the simulation conditions including the temperature will be helpful.

We also discussed the dependence of the efficiency on the target matter, in terms of the simulation of the TIP3P water molecule system. Although the accuracy is similar to the NaCl case fundamentally, the dependencies of α and l were quantitatively different in the water system. In fact, fast crossing and small-amplitude oscillations were observed in the energy error curves. These are attributed to no prominent structure in a radial direction with a long distance, mobility of the system, and relatively small atomic radii of the molecule. The last two features lead to the effect of reducing the excess subset. We explained these quantitative differences through this effect with the aid of the theoretical error analyses. However, qualitatively, the error properties are the same in general between the NaCl and water systems, as explained by the error analyses. Although the zero multipole assumption would hold at a small l in the water system, we also found that treating of a higher multipole is significantly effective to reduce the error in the radial distribution function.

The most nontrivial issue for the practical applications of the current ZM method to individual physical systems may be the setting of a suitable value of the moment l, due to the fact that the total accuracy improvement is expected when $l \leq L$, which is intrinsic to the system. Based on the error analyses and the simulation results, the following perspective is suggested. For a system where the electrostatic interactions govern the whole physical properties, the value of L tends to have a large value. In contrast, for a system where thermal kinetics or some random factor plays a prominent role than the electrostatic interactions, the value of L could have a smaller value. Roughly speaking, the former system such as the strongly-coupled ionic system prefers $l \gtrsim 3$ and the latter system such as that where many water molecules freely move prefers $l = 1$ or 2. Fortunately because the moment is a discrete parameter, its setting is finished by efforts to try $l = 1$, 2, and 3 in practice, although complete understanding and *a priori* estimation need further investigations.

We confirmed the stability of MD simulation by employing the ZM scheme with $1 \leq l \leq 4$. This property is fundamentally supported by the sufficient smoothness of the current energy function. The more stable feature with increasing the moment l conforms to the enhancement of the function smoothness with increasing l. As well as the smoothness, the energy formula takes a pairwise form and permits the atom-based cutoff mode, ensuring the exact zero total-force and so the (zero) total-momentum conservations for NVE and typical NTV equations of motion.

In the current study, we concentrated on the accuracy and stability of the method. The computational timing should be comparable to that of the ZD scheme previously developed. This is because only an even-power polynomial with respect to the atomic distance is added to the pair potential function in the ZD scheme, and the parameters of the polynomial can be evaluated preliminary to the actual step of the MD simulation. The parallel computational timing of the ZD method has already been discussed in TIP3P water system[73] and a membrane protein system,[74] and a good scalability is expected for large systems. In fact, a GPU (graphics processing unit) implementation of the ZD method enabled high speed and accurate MD simulations of soluble proteins and biomembrane

systems.[76] These are the consequence from the simple pairwise energy function formula.

As well as a MD simulation, the simplicity of the current method will be useful in a Monte Carlo calculation and a molecular modeling procedure. Applications to various systems and problems are useful to understand the relationship between the material properties and the zero-multipole assumption in a deeper way. On the other hand, interpretations from a viewpoint other than the neutrality for the ZM method may be possible and would be of value for developing cutoff-based methods.

ACKNOWLEDGMENTS

We thank Junichi Higo and Akira Kinjo for stimulating discussions and Yasushige Yonezawa for help to perform a numerical study. I.F. and H.N. were supported by Research and Development of the Next-Generation Integrated Simulation of Living Matter, a part of the Development and Use of the Next-Generation Supercomputer Project of the Ministry of Education, Culture, Sports, Science and Technology of Japan. I.F. is grateful for a Grant-in-Aid for Scientific Research (C) (25390156) from Japan Society for the Promotion of Science (JSPS), and N.K. is grateful for a Grant-in-Aid for Scientific Research (C) (25440070) from JSPS. H.N. is grateful for JSPS KAKENHI Grant Nos. 23370071 and 24118008. I.F. wishes to thank RIKEN, Japan, for an allocation of computing resources on the RIKEN Integrated Cluster of Clusters (RICC) system.

APPENDIX A: PAIRWISE-FUNCTION REPRESENTATION

The specific form of Eq. (17) for $0 \le l \le 4$ is presented as follows:

$$u^{(0)}(r) = V(r) \equiv \frac{\mathrm{erfc}(\alpha r)}{r},$$

$$u^{(1)}(r) = V(r) + \frac{1}{2}\frac{d_1}{r_c} r^2,$$

$$u^{(2)}(r) = V(r) + \left(\frac{3}{4}\frac{d_1}{r_c} + \frac{1}{4} d_2\right) r^2 - \left(\frac{1}{8}\frac{d_1}{r_c^3} + \frac{1}{8}\frac{d_2}{r_c^2}\right) r^4,$$

$$u^{(3)}(r) = V(r) + \left(\frac{15}{16}\frac{d_1}{r_c} + \frac{7}{16} d_2 + \frac{1}{16} d_3 r_c\right) r^2 - \left(\frac{5}{16}\frac{d_1}{r_c^3} + \frac{5}{16}\frac{d_2}{r_c^2} + \frac{1}{16}\frac{d_3}{r_c}\right) r^4 + \left(\frac{1}{16}\frac{d_1}{r_c^5} + \frac{1}{16}\frac{d_2}{r_c^4} + \frac{1}{48}\frac{d_3}{r_c^3}\right) r^6,$$

$$u^{(4)}(r) = V(r) + \left(\frac{35}{32}\frac{d_1}{r_c} + \frac{19}{32} d_2 + \frac{1}{8} d_3 r_c + \frac{1}{96} d_4 r_c^2\right) r^2 - \left(\frac{35}{64}\frac{d_1}{r_c^3} + \frac{35}{64}\frac{d_2}{r_c^2} + \frac{5}{32}\frac{d_3}{r_c} + \frac{1}{64} d_4\right) r^4 + \left(\frac{7}{32}\frac{d_1}{r_c^5} + \frac{7}{32}\frac{d_2}{r_c^4} + \frac{1}{12}\frac{d_3}{r_c^3} + \frac{1}{96}\frac{d_4}{r_c^2}\right) r^6 - \left(\frac{5}{128}\frac{d_1}{r_c^7} + \frac{5}{128}\frac{d_2}{r_c^6} + \frac{1}{64}\frac{d_3}{r_c^5} + \frac{1}{384}\frac{d_4}{r_c^4}\right) r^8.$$

Here

$$d_n \equiv (-)^n D^n V(r_c)$$

is $(-)^n$ times the nth derivatives of V at r_c, and its explicit form is given for any $n = 1, 2, \ldots$ as follows:

$$d_n = \frac{n!}{r_c^{n+1}} \left[\mathrm{erfc}(s) + \frac{2}{\sqrt{\pi}} \mathrm{e}^{-s^2} \sum_{m=1}^{n} \frac{1}{m!} s^m H_{m-1}(s)\right]\Bigg|_{s=\alpha r_c},$$

where $H_n(s) \equiv (-)^n \mathrm{e}^{s^2} \frac{d^n}{ds^n} \mathrm{e}^{-s^2}$ is the Hermitian polynomial with the Rodrigues representation. Namely, they are specifically given by

$$d_1 = \tfrac{1}{r_c^2}\left[\mathrm{erfc}(\alpha r_c) + \tfrac{2}{\sqrt{\pi}} \mathrm{e}^{-(\alpha r_c)^2} [\alpha r_c]\right],$$

$$d_2 = \tfrac{2}{r_c^3}\left[\mathrm{erfc}(\alpha r_c) + \tfrac{2}{\sqrt{\pi}} \mathrm{e}^{-(\alpha r_c)^2} [(\alpha r_c) + (\alpha r_c)^3]\right],$$

$$d_3 = \tfrac{6}{r_c^4}\left[\mathrm{erfc}(\alpha r_c) + \tfrac{2}{\sqrt{\pi}} \mathrm{e}^{-(\alpha r_c)^2} \left[(\alpha r_c) + \tfrac{2}{3}(\alpha r_c)^3 + \tfrac{2}{3}(\alpha r_c)^5\right]\right],$$

$$d_4 = \tfrac{24}{r_c^5}\left[\mathrm{erfc}(\alpha r_c) + \tfrac{2}{\sqrt{\pi}} \mathrm{e}^{-(\alpha r_c)^2} \left[(\alpha r_c) + \tfrac{2}{3}(\alpha r_c)^3 + \tfrac{1}{6}(\alpha r_c)^5 + \tfrac{1}{3}(\alpha r_c)^7\right]\right].$$

Thus, the parameters of the polynomial in $u^{(l)}(r)$ can be estimated prior to actual simulation steps.

APPENDIX B: UPPER BOUND OF THE EXCESS ENERGY ERROR

We derive Eq. (28) by using a continuity approximation for the particle distribution and then make relevant remarks.

The derivation can be simply and consistently done by noticing that $\mathcal{E}_i \equiv \sum_{j\in A} |\mathcal{U}^{(l)}(r_{ij})|$, where we put $A \equiv \mathcal{J}_i^{(l)}$ for simplicity, can be viewed as a value at $y = x_i$ of an extended Newtonian potential $\mathcal{E} : y \mapsto \langle \rho_A, \psi_y \rangle$. Here $\rho_A \equiv \sum_{j\in A} \delta_{(x_j)}$ is the (Schwartz) distribution of the number of the particles belonging in subset A, and we have defined a function ψ_y by $\psi_y(z) \equiv |\mathcal{U}^{(l)}(\|y - z\|)|$ for $\mathbb{R}^3 \ni z \neq y$. Namely, we have $\mathcal{E}(x_i) = \sum_{j\in A} \langle \delta_{(x_j)}, \psi_{x_i} \rangle = \sum_{j\in A} |\mathcal{U}^{(l)}(\|x_i - x_j\|)| = \mathcal{E}_i$. We approximate ρ_A by a locally integrable function

$$\rho_A^0 \equiv \rho^0 \chi_{\mathcal{A}} : y \mapsto \begin{cases} \rho^0, & \text{for } y \in \mathcal{A}, \\ 0, & \text{otherwise}, \end{cases} \tag{B1}$$

where $\mathcal{A}$ is the spherical shell inside the cutoff sphere, viz., $\mathcal{A} \equiv \{y \in \mathbb{R}^3 | \, r_c - \delta < \|y - x_i\| < r_c\}$, which mimics the

space containing the particles in the excess subset $A \equiv \mathcal{J}_i^{(l)}$ (with $0 < \delta < r_c$), and ρ^0 is a constant representing an averaged number density in $\mathcal{A}$ (e.g., $\rho^0 \sim N/V_0$ in a uniform system, where V_0 is the volume of the MD cell). Namely, the discrete-type distribution ρ_A can be approximated by the continuous-type distribution ρ_A^0, by assuming the uniformity in $\mathcal{A}$, i.e., $\#A/\mathrm{Vol}(\mathcal{A}) \sim \rho^0$ (so the total quantity is assimilated, viz., $\langle \rho_A^0, 1\rangle = \rho^0 \int_{\mathcal{A}} dy \sim \#A = \langle \rho_A, 1\rangle$, leading to a consistent description; note $\#A$ is the total number of particles in A). Thus we get

$$\begin{aligned}\mathcal{E}_i &= \langle \rho_A, \psi_{x_i}\rangle \\ &\simeq \langle \rho_A^0, \psi_{x_i}\rangle \\ &= 4\pi\rho^0 \int_{r_c-\delta}^{r_c} r^2 |\mathcal{U}^{(l)}(r)| dr,\end{aligned}$$

using the functional property of ρ_A^0 and the following integrations: $\langle \rho_A^0, \psi_{x_i}\rangle = \int_{\mathbb{R}^3} \rho_A^0(y)\psi_{x_i}(y)dy = \rho^0 \int_{\mathcal{A}} |\mathcal{U}^{(l)}(\|y - x_i\|)|dy = \rho^0 \int_{\{y\in\mathbb{R}^3 | r_c-\delta<\|y\|<r_c\}} |\mathcal{U}^{(l)}(\|y\|)|dy$.

We remark that the above estimation of the upper bound has several limitations. The estimation is based on the approximation by the continuity and uniformity regarding the excess subset. Furthermore, the signatures of the individual charges are not taken into account. Actually, as increasing r_c, even if the excess subset grows, considerable amount of cancellation with respect to $q_i q_j \mathcal{U}^{(l)}(r_{ij})$ would occur due to an increase of the variation of the particle configurations and should work to reduce the actual error values in many cases. To reduce these limitations, e.g., it may be useful to generalize Eq. (B1) as

$$\rho^0_{A_i^{(\beta)}}(y) \equiv c_i^{(\beta)} \rho_i^{(\beta)}(\|y - x_i\|)\chi_{\mathcal{A}_i^{(\beta)}}(y), \tag{B2}$$

where $\rho_i^{(\beta)}(r)$ represents a distribution function of particles that are located at a distance r from particle i and have a charge value $q^{(\beta)}$, $\mathcal{A}_i^{(\beta)}$ mimics the space containing the particles in $A_i^{(\beta)}$ that consists of particles in $\mathcal{J}_i^{(l)}$ with having a charge value $q^{(\beta)}$, and $c_i^{(\beta)}$ is a normalization constant. Here, we have still used the continuity approximation but employed the isotropy instead of the uniformity regarding $\mathcal{J}_i^{(l)}$. In this approach we have

$$\begin{aligned}\Delta_{\mathrm{exc}}(x) &= \frac{1}{2}\sum_{\alpha,\beta\in\Lambda} q^{(\alpha)} q^{(\beta)} \mathcal{E}^{(\alpha,\beta)}, \\ \mathcal{E}^{(\alpha,\beta)} &\equiv \sum_{i\in\mathcal{N}^{(\alpha)}} \mathcal{E}_i^{(\beta)}, \\ \mathcal{E}_i^{(\beta)} &\equiv \sum_{j\in A_i^{(\beta)}} \mathcal{U}^{(l)}(r_{ij}) \simeq \left\langle \rho^0_{A_i^{(\beta)}}, \psi_{x_i}\right\rangle,\end{aligned}$$

where $\mathcal{N}^{(\alpha)}$ is a set of particles having a charge value $q^{(\alpha)}$, and Λ is a set of the charge values [e.g., $\Lambda = \{-1, 1\}$ for NaCl ion system]. Although this generalization would lead to good descriptions for the cancellation stated above, it needs the information of $\rho_i^{(\beta)}$ prior to the simulation, for which $\rho_i^{(\beta)}$ depends on a system in general. In addition, a finer representation may be required in some cases. For example, δ, which is the characterization of $\mathcal{J}_i^{(l)}$, may change with increasing r_c since the counter part, viz., $\mathcal{M}_i^{(l)}$, may grow relative to the cutoff sphere with increasing r_c. To assess this, likewise, we need efforts to obtain reliable information on such a system-dependent property.

[1] M. Patra, M. Karttunen, M. T. Hyvönen, E. Falck, and I. Vattulainen, J. Phys. Chem. B **108**, 4485 (2004).
[2] M. M. Reif, V. Krautler, M. A. Kastenholz, X. Daura, and P. H. Hünenberger, J. Phys. Chem. B **113**, 3112 (2009).
[3] S. Srivastava, A. Santos, K. Critchley, K. S. Kim, P. Podsiadlo, K. Sun, J. Lee, C. Xu, G. D. Lilly, S. C. Glotzer, and N. A. Kotov, Science **327**, 1355 (2010).
[4] P. P. Ewald, Ann. Phys. (Leipzig) **369**, 253 (1921).
[5] S. W. de Leeuw, J. W. Perram, and E. R. Smith, Proc. R. Soc. London, Ser. A **373**, 27 (1980).
[6] M. Karttunen, J. Rottler, I. Vattulainen, and C. Sagui, "Electrostatics in Biomolecular Simulations: Where are we now and where are we heading?" in *Computational Modeling of Membrane Bilayers*, edited by S. E. Feller (Academic Press, Amsterdam, 2008).
[7] C. Sagui and T. A. Darden, Annu. Rev. Biophys. Biomol. Struct. **28**, 155 (1999).
[8] G. A. Cisneros, M. Karttunen, P. Ren, and C. Sagui, Chem. Rev. **114**, 779–814 (2014).
[9] A. Baumketner and J. E. Shea, J. Phys. Chem. B **109**, 21322 (2005).
[10] C. Peter, W. F. van Gunsteren, and P. H. Hünenberger, J. Chem. Phys. **119**, 12205 (2003).
[11] Y. Yonetani, J. Chem. Phys. **124**, 204501 (2006).
[12] M. Saito, J. Chem. Phys. **101**, 4055 (1994).
[13] I. Fukuda and H. Nakamura, Biophys. Rev. **4**, 161 (2012).
[14] L. Onsager, J. Am. Chem. Soc. **58**, 1486 (1936).
[15] J. A. Barker and R. O. Watts, Mol. Phys. **26**, 789 (1973).
[16] O. Steinhauser, Mol. Phys. **45**, 335 (1982).
[17] M. Neumann, Mol. Phys. **50**, 841 (1983).
[18] M. Neumann, J. Chem. Phys. **85**, 1567 (1986).
[19] M. Belhadj, H. E. Alper, and R. M. Levy, Chem. Phys. Lett. **179**, 13 (1991).
[20] P. H. Hünenberger and W. F. van Gunsteren, J. Chem. Phys. **108**, 6117 (1998).
[21] R. Gargallo, P. H. Hünenberger, F. X. Avilés, and B. Oliva, Protein Sci. **12**, 2161 (2003).
[22] R. Schulz, B. Lindner, L. Petridis, and J. C. Smith, J. Chem. Theory Comput. **5**, 2798 (2009).
[23] A. Baumketner, J. Chem. Phys. **130**, 104106 (2009).
[24] J. M. Míguez, D. González-Salgado, J. L. Legido, and M. M. Piñeiro, J. Chem. Phys. **132**, 184102 (2010).
[25] B. Ni and A. Baumketner, J. Mol. Model. **17**, 2883 (2011).
[26] E. Yakub and C. Ronchi, J. Chem. Phys. **119**, 11556 (2003).
[27] P. K. Jha, R. Sknepnek, G. I. Guerrero-García, and M. O. de la Cruz, J. Chem. Theory Comput. **6**, 3058 (2010).
[28] E. Yakub and C. Ronchi, J. Low Temp. Phys. **139**, 633 (2005).
[29] E. Yakub, J. Phys. A: Math. Gen. **39**, 4643 (2006).
[30] E. Yakub, C. Ronchi, and D. Staicu, J. Chem. Phys. **127**, 094508 (2007).
[31] G. I. Guerrero-García, P. González-Mozuelos, and M. O. de la Cruz, J. Chem. Phys. **135**, 164705 (2011).
[32] X. Wu and B. R. Brooks, J. Chem. Phys. **122**, 044107 (2005).
[33] X. Wu and B. R. Brooks, J. Chem. Phys. **131**, 024107 (2009).
[34] X. Wu and B. R. Brooks, J. Chem. Phys. **129**, 154115 (2008).
[35] K. Takahashi, T. Narumi, and K. Yasuoka, J. Chem. Phys. **133**, 014109 (2010).
[36] J. A. Te and T. Ichiye, Chem. Phys. Lett. **499**, 219 (2010).
[37] R. M. Venable, L. E. Chen, and R. W. Pastor, J. Phys. Chem. B **113**, 5855 (2009).
[38] J. B. Klauda and B. R. Brooks, J. Chem. Theory Comput. **4**, 107 (2008).
[39] J. B. Lim, B. Rogaski, and J. B. Klauda, J. Phys. Chem. B **116**, 203 (2012).
[40] H. Nakamura, T. Ohto, and Y. Nagata, J. Chem. Theory Comput. **9**, 1193 (2013).
[41] D. Wolf, Phys. Rev. Lett. **68**, 3315 (1992).
[42] D. Wolf, P. Keblinski, S. R. Phillpot, and J. Eggebrecht, J. Chem. Phys. **110**, 8254 (1999).
[43] M. B. Webb, S. H. Garofalini, and G. W. Scherer, J. Phys. Chem. B **113**, 9886 (2009).
[44] G. Jiménez-Serratos, C. Avendaño, A. Gil-Villegas, and E. González-Tovar, Mol. Phys. **109**, 27 (2011).
[45] T. S. Hofer, M. Hitzenberger, and B. R. Randolf, J. Chem. Theory Comput. **8**, 3586 (2012).

[46]Q. Wang, D. J. Keffer, S. Deng, and J. Mays, J. Phys. Chem. C **117**, 4901 (2013).
[47]Q. He, D. C. Joy, and D. J. Keffer, J. Power Sources **241**, 634 (2013).
[48]J. A. Gee, J. Chung, S. Nair, and D. S. Sholl, J. Phys. Chem. C **117**, 3169 (2013).
[49]S. F. Yang, L. M. Xiong, Q. Deng, and Y. P. Chen, Acta Mater. **61**, 89 (2013).
[50]T. Pham, K. A. Forrest, P. Nugent, Y. Belmabkhout, R. Luebke, M. Eddaoudi, M. J. Zaworotko, and B. Space, J. Phys. Chem. C **117**, 9340 (2013).
[51]A. Goyal, T. Rudzik, B. Deng, M. Hong, A. Chernatynskiy, S. B. Sinnott, and S. R. Phillpot, J. Nucl. Mater. **441**, 96 (2013).
[52]K. McLaughlin, C. R. Cioce, T. Pham, J. L. Belof, and B. Space, J. Chem. Phys. **139**, 184112 (2013).
[53]F. Ercolessi and J. B. Adams, Europhys. Lett. **26**, 583 (1994).
[54]Q. Shi, P. Liu, and G. A. Voth, J. Phys. Chem. B **112**, 16230 (2008).
[55]E. Spiga, D. Alemani, M. T. Degiacomi, M. Cascella, and M. Dal Peraro, J. Chem. Theory Comput. **9**, 3515 (2013).
[56]R. J. Petrella and M. Karplus, J. Comput. Chem. **26**, 755 (2005).
[57]Y. G. Chen and J. D. Weeks, Proc. Natl. Acad. Sci. U.S.A. **103**, 7560 (2006).
[58]L. Greengard and V. Rokhlin, J. Comput. Phys. **73**, 325 (1987).
[59]L. F. Greengard, *The Rapid Evaluation of Potential Fields in Particle Systems* (MIT Press, Cambridge, 1988).
[60]G. Mathias, B. Egwolf, M. Nonella, and P. Tavan, J. Chem. Phys. **118**, 10847 (2003).
[61]T. N. Heinz and P. H. Hünenberger, J. Chem. Phys. **123**, 034107 (2005).
[62]Y. Lin, A. Baumketner, S. Deng, Z. Xu, D. Jacobs, and W. Cai, J. Chem. Phys. **131**, 154103 (2009).
[63]Y. Lin, A. Baumketner, W. Song, S. Deng, D. Jacobs, and W. Cai, J. Chem. Phys. **134**, 044105 (2011).
[64]S. A. Hassan, J. Phys. Chem. B **111**, 227 (2007).
[65]P. Demontis, S. Spanu, and G. B. Suffritti, J. Chem. Phys. **114**, 7980 (2001).
[66]D. Zahn, B. Schilling, and S. M. Kast, J. Phys. Chem. B **106**, 10725 (2002).
[67]M. C. C. Ribeiro, J. Phys. Chem. B **107**, 9520 (2003).
[68]C. Avendaño and A. Gil-Villegas, Mol. Phys. **104**, 1475 (2006).
[69]C. J. Fennell and J. D. Gezelter, J. Chem. Phys. **124**, 234104 (2006).
[70]I. Fukuda, Y. Yonezawa, and H. Nakamura, J. Phys. Soc. Jpn. **77**, 114301 (2008).
[71]Y. Yonezawa, I. Fukuda, N. Kamiya, H. Shimoyama, and H. Nakamura, J. Chem. Theory Comput. **7**, 1484 (2011).
[72]I. Fukuda, Y. Yonezawa, and H. Nakamura, J. Chem. Phys. **134**, 164107 (2011).
[73]I. Fukuda, N. Kamiya, Y. Yonezawa, and H. Nakamura, J. Chem. Phys. **137**, 054314 (2012).
[74]N. Kamiya, I. Fukuda, and H. Nakamura, Chem. Phys. Lett. **568–569**, 26 (2013).
[75]T. Arakawa, N. Kamiya, H. Nakamura, and I. Fukuda, PLoS One **8**, e76606 (2013).
[76]T. Mashimo, Y. Fukunishi, N. Kamiya, Y. Takano, I. Fukuda, and H. Nakamura, J. Chem. Theory Comput. **9**, 5599 (2013).
[77]I. Fukuda, J. Chem. Phys. **139**, 174107 (2013).
[78]M. P. Tosi and F. G. Fumi, J. Phys. Chem. Solids **25**, 45 (1964).
[79]Y. Fukunishi, Y. Mikami, and H. Nakamura, J. Phys. Chem. B **107**, 13201 (2003).
[80]U. Essmann, L. Perera, M. L. Berkowitz, T. Darden, H. Lee, and L. G. Pedersen, J. Chem. Phys. **103**, 8577 (1995).
[81]W. L. Jorgensen, J. Chandrasekhar, J. D. Madura, R. W. Impey, and M. L. Klein, J. Chem. Phys. **79**, 926 (1983).
[82]P. Keblinski, J. Eggebrecht, D. Wolf, and S. R. Phillpot, J. Chem. Phys. **113**, 282 (2000).
[83]T. G. Desai, J. Chem. Phys. **127**, 154707 (2007).
[84]T. C. Bishop, R. D. Skeel, and K. Schulten, J. Comput. Chem. **18**, 1785 (1997).
[85]A. Neelov and C. Holm, J. Chem. Phys. **132**, 234103 (2010).
[86]P. J. Steinbach and B. R. Brooks, J. Comput. Chem. **15**, 667 (1994).
[87]R. D. Skeel, D. J. Hardy, and J. C. Phillips, J. Comput. Phys. **225**, 1 (2007).